

Observations and scaling of the atmospheric boundary layer

G.D. Hess

Bureau of Meteorology Research Centre, Australia

(Manuscript received April 1992; revised July 1992)

One of the areas of research that Reg Clarke took a particular interest in was the atmospheric boundary layer (ABL). In this review we examine observations of the structure of the ABL based on a framework of similarity scaling. This includes: the Monin-Obukhov surface layer; the free-convection layer; the near-neutral upper layer; the mixed layer; the stable layer scaled by local fluxes; and the stable intermittent layer. Limitations of this framework are illustrated for the horizontal wind variances in the surface layer and the moisture flux in the mixed layer. Recent developments in prescribing surface layer stable profiles, top-down bottom-up scaling for the mixed layer, free-convection fluxes, generalised Rossby number similarity theory, and treatment of inhomogeneous surfaces are emphasised.

Introduction

Reg Clarke's name is synonymous with Australian studies of the atmospheric boundary layer (ABL). The ABL is the region of the atmosphere near the surface where small-scale turbulent transfer processes are important. Knowledge of its behaviour is essential for many practical problems from air pollution studies to climate modelling. Reg designed, organised and led a number of major field programs in the 1960s and 70s to observe the structure of the ABL under a wide range of stability conditions. These included expeditions at Kerang, Victoria, in 1964 and Hay, NSW, in 1965 (Clarke (1970), the pre-Wangara experiments); at Hay, NSW, in 1967 (Clarke et al. (1971), the Wangara Experiment) and Daly Waters, NT, in 1974 (Clarke and Brook (1979), the Koorin Experiment). These studies have become classical experiments, providing researchers with a rich source of high quality data.

The pre-Wangara and Wangara Experiments were conducted over flat, relatively smooth terrain (roughness length $z_0 \approx 0.001 - 0.005$ m) in middle latitudes (34.5 and 35.8°S); the Koorin Experiment was conducted over savannah land covered by trees ($z_0 \approx 0.5$ m) at a low latitude (16°S). However even over a site, such as the Wangara site, carefully chosen to simplify the data interpretation, the atmosphere is often very

complex (particularly under stable conditions) because of unsteadiness, inhomogeneities, accelerations, baroclinicity and intermittency. Most researchers have restricted their studies of the Wangara data to Day 33, a day dominated by thermal convection with little advection. (It should be noted in this regard that both the Wangara and the Koorin Experiments were conducted in winter-time, whereas the classical boundary layer experiments conducted in the United States, i.e. the Great Plains Experiment, the Kansas Experiment and the Minnesota Experiment, were conducted in the summertime.)

The main emphasis in Reg's ABL experiments was on mean profile measurements in the outer layer combined with momentum, heat and moisture flux estimates in the surface layer, estimates of surface roughness lengths and measurements of the horizontal gradients of surface pressure and temperature. In the early experiments the surface flux estimates were derived from mean profile measurements from masts and were checked with measurements of ground flux and net radiation and use of the equation for surface energy balance. As the electronics improved, direct eddy correlation measurements of the fluxes were introduced. During the Wangara Experiment preliminary eddy correlation measurements were made in the surface layer on five days. By the time of the Koorin Experiment eddy correlation measurements were routinely carried out in the surface layer and on two days eddy correlation

Corresponding author address: G.D. Hess, Bureau of Meteorology Research Centre, GPO Box 1289K, Melbourne, Vic 3001, Australia.

measurements of heat flux were made in the outer layer from an instrumented aircraft.

Reg's experiments had a significant impact on ABL research. The results appeared just at the time when advances in computer technology were making it possible to carry out sophisticated numerical simulations of the ABL (higher-order closure models and large-eddy simulations). The observations from his experiments gave a touchstone with reality.

In this paper we shall present an overview of some of the progress made in understanding the ABL in the 25 years since the Wangara Experiment. This review is by necessity selective rather than comprehensive, emphasising observations and scaling. Readers interested in learning more about the ABL are referred to a number of excellent recent textbooks dealing with the atmospheric boundary layer (Arya 1988; Stull 1988; Sorbjan 1989; Garratt 1992), general surveys on the ABL (Friehe 1987; Kaimal 1988; Wyngaard 1985, 1988b) and more specific surveys, such as the convective boundary layer (Young 1988a,b,c,d; Wyngaard 1988a), the stable boundary layer (Hunt 1985), the marine boundary layer (LeMone 1980; Businger 1985; Joffre 1985), problems in the ABL and the evaluation of models (Wyngaard 1990a,b), scalar structure in the ABL (Webb 1984; Wyngaard 1990c), cloud-topped boundary layers (WMO 1985; Driedonks and Duynkerke 1989), measurement techniques (Lenschow 1986), mixed-layer models (Deardorff 1980; Driedonks 1982; Manins 1982), the internal boundary layer (Garratt 1990), diffusion in the ABL (Weil 1988; Venkatram 1988a, 1988b), higher-order closure modelling of the ABL (Zeman 1981; Mellor and Yamada 1982; Holt and Raman 1988), large-eddy simulation (Wyngaard 1984), air-land interaction (ECMWF 1989; Brutsaert 1982) and air-sea interaction (Smith 1988, 1989; Geernaert and Plant 1990; Donelan 1990). Readers also should consult the extremely valuable earlier reviews (Monin and Yaglom 1971, 1975; Haugen 1973; Wippermann 1973; Deardorff 1978; Blackadar 1979; McBean 1979; Nieuwstadt and van Dop 1982; Wyngaard 1983; Panofsky and Dutton 1984).

The role of observations has been a key element in promoting our understanding of the ABL. Hess et al. (1981) and Garratt and Hicks (1990) discuss the goals and underlying philosophy, the main results and some of the problems encountered in five major Australian micrometeorological and ABL expeditions. Similar discussions for other important ABL experiments are: Lettau (1990), the Great Plains Experiments; Kaimal and Wyngaard (1990), the Kansas and Minnesota Experiments; André et al. (1990), the HAPEX-MOBILHY Experiment; Betts et al. (1990), the FIFE Experiment; Hasse (1990), marine boundary-layer experiments; and Panin (1990), air-sea

interaction experiments in the USSR. A partial list of boundary-layer experiments is given by Stull (1988, pp. 418–19). Reg's own interest in the ABL continued until his death; his last three papers (Clarke 1990a,b,c), published posthumously, deal with observations and modelling of the Koorin Experiment.

ABL scaling

Scaling is a technique used to help present and interpret ABL data. Under steady, barotropic, horizontally homogeneous, clear sky conditions it is assumed that the ABL can be characterised by a few physical parameters. When atmospheric data, such as the differences in mean values at two heights, variances, covariances, gradients, turbulent diffusivities, spectra and cospectra, etc., are made non-dimensional by appropriate powers of the characteristic parameters, plots of the data versus non-dimensional height should be functions only of the thermal stability.

Important parameters governing the processes near the surface are the buoyancy flux $F_B = (g/\Theta_v)\overline{w\theta_{0v}}$ and the momentum flux $\tau_0 = \rho u_*^2$, where g is the acceleration due to gravity, w the fluctuating vertical velocity, θ_v and Θ_v are the fluctuating and mean virtual potential temperature, respectively, ρ is the air density and u_* the friction velocity. Other important scaling factors are the height above the surface z and the height of the turbulent layer h . When F_B is positive h is often limited by the base of a capping inversion.

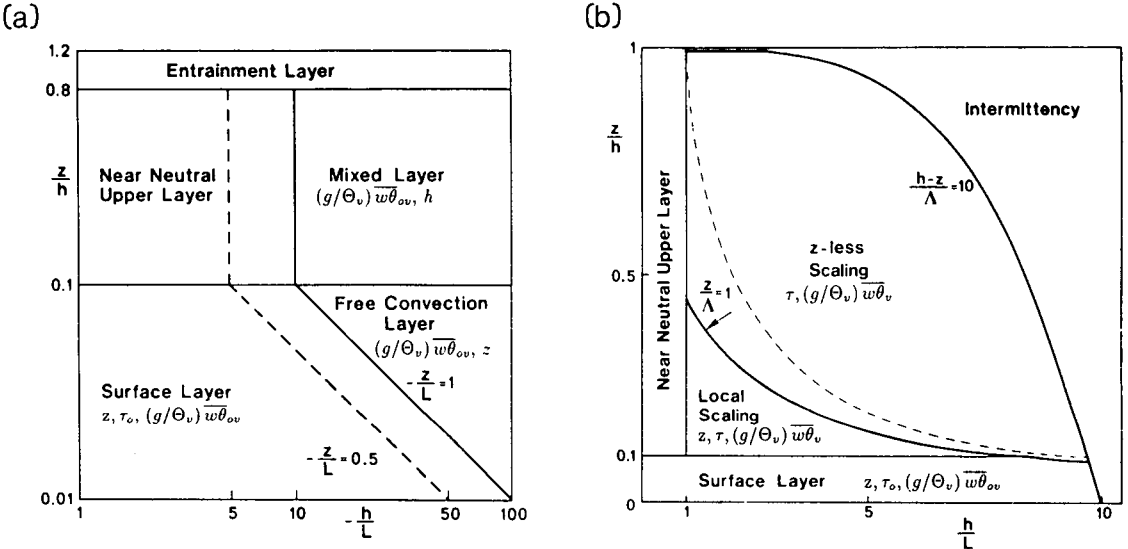
The thermal stability in the surface layer ζ is given by the ratio of the height z to the Obukhov length L , i.e. $\zeta = z/L$, where L is given by

$$L = -u_*^3 / (kg/\Theta_v)\overline{w\theta_{0v}} \quad \dots 1$$

where k is the von Kármán constant. The thermal stability for the whole boundary layer is given by the ratio h/L .

A number of authors (Deardorff 1978; Nicholls and Readings 1979; van Dop et al. 1980; Olesen et al. 1984) have developed classification schemes for ABL scaling. In Fig. 1 we show the scheme proposed by Holtslag and Nieuwstadt (1986). For positive buoyancy flux (Fig. 1(a)) the surface layer extends to $z/h \cong 0.1$ and the physical parameters of significance are z , τ_0 , (g/Θ_v) and $\overline{w\theta_{0v}}$ (for dry air $\overline{w\theta_{0v}}$ becomes $\overline{w\theta_0}$). These are the scaling parameters of the Monin and Obukhov (1954) similarity theory. As the surface layer becomes more unstable the importance of buoyancy flux increases and momentum flux decreases. Eventually the momentum flux is no longer an important parameter and the layer is said to follow free convection scaling. Holtslag and Nieuwstadt suggest that the transition from surface layer scaling to free convection scaling occurs between $-h/L \cong 5$ to 10. The demarcation between the regimes is

Fig. 1 Schematic diagram indicating ABL scaling regions and physical parameters of importance. (a) Unstable case (positive buoyancy, $L < 0$). Instability increases as $-h/L$ increases. The dashed and solid lines indicate the transition region to the convective state. (b) Stable case (negative buoyancy, $L > 0$). Stability increases as h/L increases. The dashed line is prescribed by $z/L = 1$. Comparison of the dashed and solid lines shows where the local length-scale Λ is approximately equal to the Obuhkov length L based on surface fluxes (after Holtslag and Nieuwstadt (1986)).



gradual and other authors (see below) choose different limits.

For $0.1 < z/h < 0.8$ and $-h/L < 5$ to 10 the layer is near neutral. In this region the height of the inversion h and the Monin–Obukhov (M–O) surface layer parameters are important. For $-h/L > 10$ free convection scaling is modified to mixed layer scaling by replacing z with h .

The region $0.8 \leq z/h \leq 1.2$ is called the entrainment region. In this zone the warm air from the capping inversion mixes with the boundary-layer air and the simple scaling scheme, described above, does not apply. We shall return to this region later when we discuss the top-down and bottom-up diffusion in the section on mixed-layer similarity scaling.

When the buoyancy flux is negative the flow is stably stratified (see Fig. 1(b)). Again we have a Monin–Obukhov surface layer and a near-neutral upper layer. In the region above the surface layer Monin–Obukhov scaling applies, providing that local values of the fluxes are used. The length scale Λ plays the role of L and is defined as in Eqn 1 except that the surface fluxes τ_0 and $\overline{w\theta_{ov}}$ are replaced by local values τ and $\overline{w\theta_v}$. As the flow becomes more stable the height above the surface becomes less important. At very great stability the turbulence becomes intermittent.

The viscous sublayer at the surface (see Brutsaert 1982; Garratt 1992) is not shown in Fig. 1. In the sections below we consider each of the

regions of Fig. 1 separately. Because of the limitations of space, spectra and cospectra, structure functions, structure parameters and most of the budgets of turbulent fluxes and variances are not discussed (see Stull (1988), Sorbjan (1989), Garratt (1992), for example).

Monin–Obukhov surface-layer scaling

Based on the M–O parameters, scales for non-dimensionalising the velocity, temperature and humidity can be defined as:

$$u_* \equiv (\tau_0/\rho)^{1/2}, T_{*v} \equiv -\overline{w\theta_{0v}}/u_*, \text{ and} \quad \dots 2$$

$$q_* \equiv -\overline{wq_0}/u_*$$

where q is the fluctuating specific humidity. The surface-layer gradients can be written in non-dimensional form as:

$$\phi_M(\zeta) = (kz/u_*) \partial U/\partial z \quad \dots 3$$

$$\phi_H(\zeta) = (kz/T_{*v}) \partial \Theta_v/\partial z \quad \dots 4$$

$$\phi_Q(\zeta) = (kz/q_*) \partial Q/\partial z \quad \dots 5$$

where U , Θ_v and Q indicate mean values of the wind speed, virtual potential temperature and specific humidity, respectively. Observations (mainly over land) show that for passive scalars the M–O non-dimensional gradients are equal, i.e. $\phi_Q(\zeta) = \phi_H(\zeta)$.

Other relevant quantities in describing the dynamics of the surface layer are the dissipation of turbulent kinetic energy ϵ , the standard deviation of w (denoted σ_w), and the standard deviation of θ_v (denoted σ_{θ_v}). Their non-dimensional forms are:

$$\phi_\epsilon(\zeta) = (kz\epsilon/u_*^3) \quad \dots 6$$

$$\phi_w(\zeta) = \sigma_w/u_* \quad \dots 7$$

$$\phi_{\theta_v}(\zeta) = \sigma_{\theta_v}/|T_{*v}| \quad \dots 8$$

The standard deviations of the horizontal wind components u and v do not obey M-O scaling and will be discussed later.

The functional forms for Eqns 3 to 8 ultimately must be determined experimentally. Kaimal (1988) has re-analysed the Kansas data (Businger et al. 1971; Wyngaard and Coté 1971). Based on these observations and those summarised by Dyer (1974) and Högström (1988) he recommends the following:

$$\phi_M = \begin{cases} (1 - 16 z/L)^{-1/4} & -2 \leq z/L \leq 0 \\ (1 + 5 z/L) & 0 \leq z/L \leq 1 \end{cases} \dots 9(a) \text{ and } (b)$$

$$\phi_H = \phi_Q = \begin{cases} (1 - 16 z/L)^{-1/2} & -2 \leq z/L \leq 0 \\ (1 + 5 z/L) & 0 \leq z/L \leq 1 \end{cases} \dots 10(a) \text{ and } (b)$$

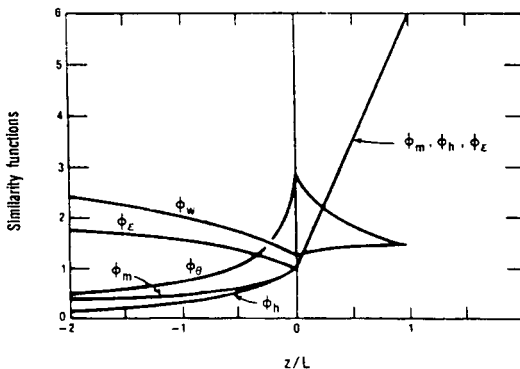
$$\phi_\epsilon = \begin{cases} (1 + 0.5|z/L|^{2/3})^{3/2} & -2 \leq z/L \leq 0 \\ (1 + 5 z/L) & 0 \leq z/L \leq 1 \end{cases} \dots 11(a) \text{ and } (b)$$

$$\phi_w = \begin{cases} 1.25 (1 - 3 z/L)^{1/3} & -2 \leq z/L \leq 0 \\ 1.25 (1 + 0.2 z/L) & 0 \leq z/L \leq 1 \end{cases} \dots 12(a) \text{ and } (b)$$

$$\phi_{\theta_v} = \begin{cases} 3 (1 - 16 z/L)^{-1/2} & -2 \leq z/L \leq 0 \\ 3 (1 + z/L)^{-1} & 0 \leq z/L \leq 1 \end{cases} \dots 13(a) \text{ and } (b)$$

These formulations assume that $k \approx 0.4$ (see e.g., Zhang et al. 1988) and the neutral turbulent Prandtl number Pr is unity, i.e. $\phi_H(0)/\phi_M(0) = 1$. The formulations of other investigators have been summarised by Sorbjan (1989, pp. 74-6). The M-O similarity functions given by Eqns 9 to 13 are plotted in Fig. 2.

Fig. 2 Monin-Obukhov similarity functions $\phi_M, \phi_H, \phi_Q = \phi_H, \phi_{\theta_v}, \phi_\theta = \phi_{\theta_v}, \phi_w$ and ϕ_ϵ as a functions of stability z/L (after Kaimal (1988)).



Integration of Eqns 9 and 10 formally can be written as:

$$k (U - U_0)/u_* = \ln(z/z_0) - \Psi_M(z/L) + \Psi_M(z_0/L) \quad \dots 14$$

$$k (\Theta_v - \Theta_{0v})/T_{*v} = \ln(z/z_H) - \Psi_H(z/L) + \Psi_H(z_H/L) \quad \dots 15$$

$$k (Q - Q_0)/q_* = \ln(z/z_Q) - \Psi_Q(z/L) + \Psi_Q(z_Q/L) \quad \dots 16$$

where $U_0 = 0$ over land; over the sea the surface drift current U_0 is $O(u_*)$.

The parameters z_0, z_H and z_Q are the roughness lengths for momentum, heat and moisture, respectively. For large roughness elements a zero-plane displacement needs to be introduced to account for the canopy effect. The roughness lengths are determined by extrapolating the M-O profiles downward and finding the heights above the zero-plane displacement at which the surface values U_0, Θ_0 and Q_0 are obtained. Equations 14 to 16 lose accuracy below heights about 100 times the roughness length (Garratt 1980).

Although it is generally accepted that $z_Q = z_H$ over land, $z_0 \neq z_H$. Measurements over homogeneous, densely packed, vegetated surfaces typically indicate that $z_H \approx z_0/10$ (see e.g., Garratt and Hicks 1973; Brutsaert 1982). Recently Beljaars and Holtslag (1991) have found that $z_H \approx z_0/(6.4 \times 10^3)$ for the flat grassland at the Cabauw tower in Holland (with a minimum of a 200 m, apparently uniform, fetch in all directions). They obtained a similar value based on the MESOG-ERS-84 data (southern France), using surface radiation temperature measurements from aircraft flights. Their results correspond to a temperature difference of up to 6K between the heights z_0 and z_H . Beljaars and Holtslag attribute this large temperature jump to mesoscale inhomogeneities. We shall return to this topic later.

Over the sea the roughness lengths are given by simple interpolation formulas between rough flow over gravity waves and smooth flow (Charnock 1855; Smith 1988, 1989; Liu et al. 1979; Godfrey and Beljaars 1991)

$$z_0 = \alpha u_*^2/g + a_U v/u_* \quad \dots 17$$

$$z_H = 1.4 \times 10^{-5} + a_T v/u_* \quad \dots 18$$

$$z_Q = 1.3 \times 10^{-4} + a_Q v/u_* \quad \dots 19$$

where v is the kinematic viscosity of air and $\alpha = 0.011$ for open ocean. Smith suggests that the higher values of α obtained earlier by Garratt (1977) ($\alpha = 0.014$ for $k = 0.41$; $\alpha = 0.017$ for $k = 0.4$) and Wu (1980) ($\alpha = 0.0185$) reflect data with limited fetch and depth. In Eqn 17 $a_U = 0.11$, but the values of a_T and a_Q in Eqns 18 and 19 are uncertain; they lie in the range 0.2 to 0.6. More complex relations for z_0 , depending on the sea state are discussed by Donelan (1990).

In Eqns 14 to 16 the profile stability corrections are given by (Paulson 1970):

$$\Psi_M = \begin{cases} 2 \ln(1+x) + \ln(1+x^2) - 2 \tan^{-1}x & -2 \leq z/L \leq 0 \\ -5 \zeta & 0 \leq z/L \leq 1 \end{cases} \dots 20 \text{ (a)}$$

$$\dots 20 \text{ (b)}$$

$$\Psi_H = \Psi_Q = \begin{cases} 2 \ln(1+x^2) & -2 \leq z/L \leq 0 \\ -5 \zeta & 0 \leq z/L \leq 1 \end{cases} \dots 21 \text{ (a)}$$

$$\dots 21 \text{ (b)}$$

where $x \equiv (1 - \gamma \zeta)^{1/4}$, $\gamma \approx 16$, and ζ is the argument of the Ψ functions (z/L , z_0/L , z_H/L or z_Q/L). If $z_0, z_H, z_Q \ll L$ then at the roughness length limit $x \approx 1$, Eqn 20(a) yields $\Psi_M(z_0/L) \approx 3 \ln 2 - \pi/2$ and Eqn 21(a) yields $\Psi_H(z_H/L) = \Psi_Q(z_Q/L) \approx 2 \ln 2$.

Webb (1970) and Hicks (1976) find that the profiles in stable conditions deviate from the log-linear form of Eqn 20(b) and Eqn 21(b) for $z/L > 0.5$. As the stability increases the turbulence becomes more intermittent and the exchange processes for heat and momentum become dissimilar ($\phi_H > \phi_M$). Beljaars and Holtslag (1991) suggest the following relations for stable conditions, based on Cabauw tower data, to account for profile dissimilarity:

$$-\Psi_M = a z/L + b (z/L - cd) \exp(-d z/L) + b cd \dots 22$$

$$-\Psi_H = (1 + 2a z/3L)^{3/2} + b (z/L - cd) \exp(-d z/L) + b cd - 1 \dots 23$$

where $a = 1.0$, $b = 0.667$, $c = 5$, $d = 0.35$. They find that Eqns 22 and 23 can be extended well above the surface layer and seem to incorporate the relationship between the local and surface fluxes. At large values of z/L these relations yield a flux Richardson number ($R_f \equiv (z/L) \phi_M^{-1}$) which approaches a constant.

Equations 14 to 16 are usually solved iteratively (e.g. Delsol et al. 1971) or by approximation by fitting functions (Louis 1979). Recently analytical, approximate and regression solutions have been obtained for special cases by Choudhury et al. (1986), Byun (1990) and Viney (1991).

Free convection

In the free convection layer the buoyancy flux is positive and large and the winds are light. The scales for velocity, temperature and humidity are:

$$u_f \equiv ((g/\Theta_v) \overline{w\theta_{0v}z})^{1/3}, \Theta_f \equiv \overline{w\theta_{0v}}/u_f \text{ and } q_f \equiv \overline{wq_0}/u_f \dots 24$$

Since the available scales cannot be combined to form a non-dimensional height, all non-dimensional quantities should be constant. For example, Wyngaard and Coté (1971) find

$$\sigma_w/u_f = 1.8 \text{ and } \sigma_{\theta_v}/\Theta_f = 0.95 \dots 25$$

The non-dimensional eddy diffusivities become $K_M/u_f z = \text{constant}$, $K_H/u_f z = \text{constant}$ and the non-dimensional wind and potential temperature gradients become $(u_f/u_*')^2 (kz/u_f) (\partial U/\partial z) = \text{constant}$ and $(kz/\Theta_f) (\partial \Theta_v/\partial z) = \text{constant}$; hence

$$\phi_M(\zeta) \sim \phi_H(\zeta) \sim \phi_Q(\zeta) \sim (-\zeta)^{-1/3} \dots 26$$

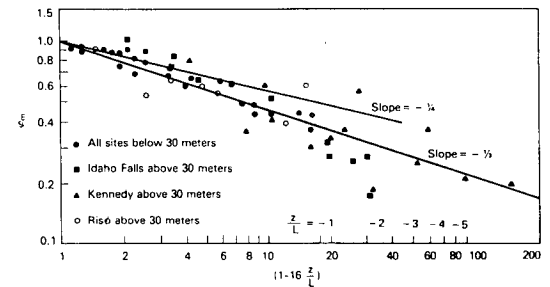
$$\phi_\theta(\zeta) = -0.35 \zeta \dots 27$$

$$\phi_w(\zeta) = 1.8 (-\zeta)^{1/3} \dots 28$$

$$\phi_{\theta_v} = 0.95 (-\zeta)^{-1/3} \dots 29$$

Note that Eqns 9(a), 10(a) and 13(a) are empirical equations for data in the range $-2 \leq \zeta \leq 0$ and do not have the correct asymptotic form for free convection. In Fig. 3 we show some preliminary results for the stability dependence of ϕ_M in very unstable conditions, illustrating the changeover from Eqn 9(a) to Eqn 26 (Carl et al. 1973). As $\zeta \rightarrow -\infty$ the gradients become small and measurements are difficult. The ϕ functions in this region have not been adequately documented experimentally.

Fig. 3 Non-dimensional wind shear ϕ_M as a function of stability for very unstable conditions (after Carl et al. (1973)).



We now turn our attention to light wind, highly convective conditions over the sea. The fluxes can be parametrised by introducing bulk transfer coefficients, C_D , C_H and C_E :

$$\tau_0 = \rho C_D (U - U_0)^2 \dots 30$$

$$H_0 = \rho c_p C_H (U - U_0) (\Theta_0 - \Theta) \dots 31$$

$$E_0 = \rho C_E (U - U_0) (Q_0 - Q) \dots 32$$

where C_D , C_H and C_E have been found in moderate wind speeds to be constant or a linear function of wind speed (e.g. Smith 1988). We can write explicit relations for the bulk transfer coefficients, using Eqns 14 to 16

$$C_D \equiv [u_* / (U - U_0)]^2 = k^2 / (\ln(z/z_0) - \Psi_M(z/L) + \Psi_M(z_0/L))^2 \quad \dots 33$$

$$C_H \equiv (H_0 / \rho c_p (U - U_0)) / (\Theta_0 - \Theta) = k C_D^{1/2} / (\ln(z/z_H) - \Psi_H(z/L) + \Psi_H(z_H/L)) \quad \dots 34$$

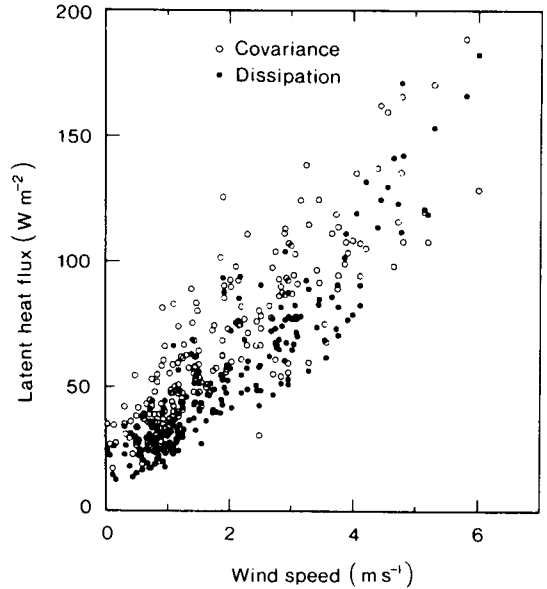
$$C_E \equiv (E_0 / \rho (U - U_0)) / (Q_0 - Q) = k C_D^{1/2} / (\ln(z/z_Q) - \Psi_Q(z/L) + \Psi_Q(z_Q/L)) \quad \dots 35$$

where the reference height for U , Θ and Q is usually taken to be 10 m. In the literature it is common to specify the bulk transfer coefficients relative to their values at neutral stability (C_{DN} , C_{HN} and C_{EN}), i.e. where the sums of the Ψ functions in Eqns 33 to 35 are each zero.

Bradley et al. (1991) present what appear to be among the first published direct flux measurements covering the wind speed range 0–4 m s⁻¹ over open ocean (also see Golitsyn and Grachov (1986)). Their results show that the fluxes do not go to zero as the relative mean wind speed goes to zero, and hence the bulk transfer coefficients in this light-wind regime are no longer constant or linearly increasing with wind speed. Figure 4 shows the latent heat flux determined from their covariance measurements (expressed as E_0 , where is the latent heat of vapourisation). When the measurements are extrapolated to zero wind speed, the latent heat flux has a value of about 25 W m⁻²; the results from the inertial dissipation method give about 20 W m⁻². In the long term this flux at zero wind speed represents a significant transfer of energy not included by use of the bulk transfer forced convection equations.

Hicks (1975), Kondo (1975), Liu et al. (1979), and Miller et al. (1992) have developed models to account for the role of the molecular surface layer in computing the fluxes at low wind speeds. To test these models Bradley et al. (1991) have measured bulk coefficients at sea in free convection conditions (using $\gamma \cong 28$ in Eqn 20(a) and $\gamma \cong 14$ in Eqn 21(a) based on Dyer and Bradley (1982)). They compared their measurements with the predictions of C_D , C_H and C_E of Liu et al. (1979) and C_{DN} , C_{HN} and C_{EN} of Kondo (1975). The measured drag coefficient C_D (not shown) is higher than the predictions of Liu et al., but lower than the empirical relation developed by Geernaert et al. (1988), using data at higher wind speeds. In Fig. 5 we show their results for C_{HN} and C_{EN} . The agreement between observations and the Liu et al. model is excellent for C_E ; the agreement is less good for C_H but the heat flux is relatively small and there is more scatter in the data. In each case for $(U - U_0) < 2$ m s⁻¹, as the wind speed goes to zero the bulk transfer coefficient increases, confirming the predicted trend in the models. Similar experimental results have been obtained by Chris Fairall (personal communication).

Fig. 4 Latent heat flux ($\mathcal{L} E_0$) as a function of wind speed. The open circles indicate covariance measurements and the filled circles are estimates based on the inertial dissipation technique. Note that the latent heat flux does not go to zero at zero wind speed because of convective motions (after Bradley et al. (1991)).



Godfrey and Beljaars (1991) extend the model of Hicks-Kondo-Liu et al.-Miller et al. They multiply the right hand side of Eqns 15 and 16 by 0.88 (i.e. they assume $\phi_H(0)/\phi_M(0) = \phi_Q(0)/\phi_M(0) = 0.88$ rather than 1). They then evaluate Eqns 14 to 19 and Eqns 20(a) to 21(a) for low wind conditions and obtain the following expressions for the buoyancy flux F_B , the latent and sensible heat fluxes, and the momentum flux:

$$F_B = v^{1/3} (\Delta B)^{4/3} G(\xi) \quad \dots 36$$

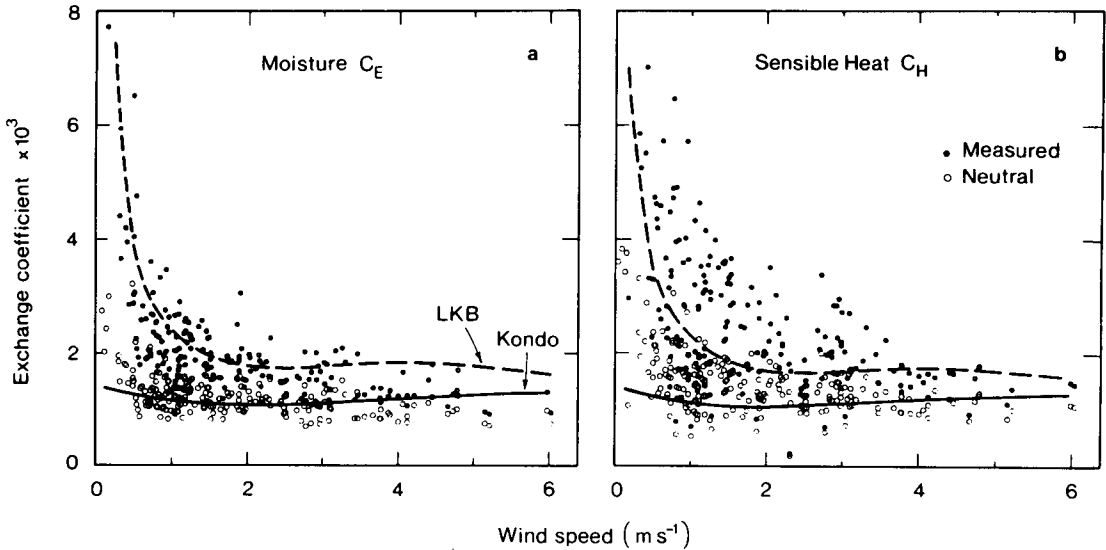
$$\mathcal{L} E_0 = (\rho \mathcal{L} (Q - Q_0) / \Delta B) F_B \quad \dots 37$$

$$H_0 = (\rho c_p (\Theta - \Theta_0) / \Delta B) F_B \quad \dots 38$$

$$(U - U_0)^3 / \nu \Delta B = 7.10 \xi (\ln(C_0 \xi))^3 / \ln(C_1 \xi) \quad \dots 39$$

where $\Delta B \equiv (g/\Theta_v) (\Theta_v - \Theta_{0v})$, $G(\xi) \equiv \xi^{1/3} / (2.2 \ln(C_1 \xi))$, $\xi \equiv -u_*^3 / (\nu (g/\Theta_v) T_{*v})$, $C_0 \equiv 96.2 / \gamma a_U$ and $C_1 \equiv 10 / \gamma a_T$. Their algorithm is not applicable for $\xi \leq 41.4$ (which roughly corresponds to a wind speed of 0.3 m s⁻¹). This limit is at the minimum in the $G(\xi)$ curve. At this limit $G(\xi) = 0.191$ and Eqns 36 to 38 are in good agreement with results obtained in an independent manner for zero-wind laboratory experiments (Golitsyn and Grachov 1986); hence we set $G(\xi) = 0.191$ for $\xi \leq 41.4$

Fig. 5 Eddy-correlations measurements of the bulk transfer coefficients for (a) water vapour C_E and C_{EN} and (b) sensible heat C_H and C_{HN} . The measurements are compared with model predictions by Liu et al. (1979) (long-dashed curve) for C_E and C_H , and Kondo (1975) (solid line curve) for C_{EN} and C_{HN} (after Bradley et al. (1991)).



Similar calculations could be carried out for ϕ functions proposed by Carl et al. (1973) which obey the free convection limit.

There are singularities at $\xi = 1/C_0$ and $1/C_1$ in Eqn 39) but in the atmosphere these are probably never encountered. Atmospheric convective downdrafts create horizontal wind fluctuations even if the mean wind approaches zero (Deardorff 1972; Businger 1973; Schumann 1988; Schmidt and Schumann 1989; Miller et al. 1992). These fluctuations scale with the mixed-layer convective velocity, w_* :

$$w_G = \beta w_* \quad \dots 40$$

where $w_* \equiv [(g/\Theta_v) \overline{w\theta}_{0v} h]^{1/3}$ and β is a constant for dry convection Deardorff (1972) finds $\beta = 0.7$, while Miller et al. (1992) use $\beta = 1$; for moist convection the parametrisation problem is more complex and has not yet been solved). Godfrey and Beljaars (1991) suggest that β should be adjusted to maximise model agreement with observations. They note that replacing $(U - U_0)$ with $((U - U_0)^2 + w_G^2)^{1/2}$ in Eqn 39 automatically removes the low wind speed singularity for boundary-layer depths of ~ 1000 m or greater.

Near-neutral upper layer scaling

The ABL over the sea is cooler and less convective than over land and often falls into the near-neutral category for $z > 0.1 h$. This category also applies over land when there are strong winds or when the elevation angle of the sun is very low. In this layer mechanical mixing is important even at large values of z/h . Hence the velocity, temperature and humidity scale as in the M-O surface layer (i.e. with u_* , T_{*v} and q_*), but the height h is also a relevant scale.

Nicholls and Readings (1979) present observations over the sea for two stability classes (see Fig. 6). The average stability of the circles is $-h/L = 0.9$ and of the triangles is $-h/L = 3.9$. The profiles are limited to $z/h < 0.7$ to minimise the effects of clouds and entrainment processes. The U profile shows the effect of greater mixing (less momentum defect) for increased instability while the V profile is unchanged in the two classes. The potential temperature lapse rate closely approximates the dry adiabatic rate, but the specific humidity decreases linearly with height indicating

Fig. 6 Non-dimensional mean profiles for (a) U/u_* , (b) V/u_* , (c) $(\Theta - \Theta_{10})$ and (d) $(Q - Q_{10})$ in near-neutral conditions. The subscript 10 indicates that the quantity is evaluation at 10 m height. The height z_1 is inversion height (i.e. $z_1 = h$). The circles denote near-neutral values (average $-h/L = 0.9$); the triangles denote slightly unstable values (average $-h/L = 3.9$); error bars indicate the standard error of the mean (after Nicholls and Readings (1979)).

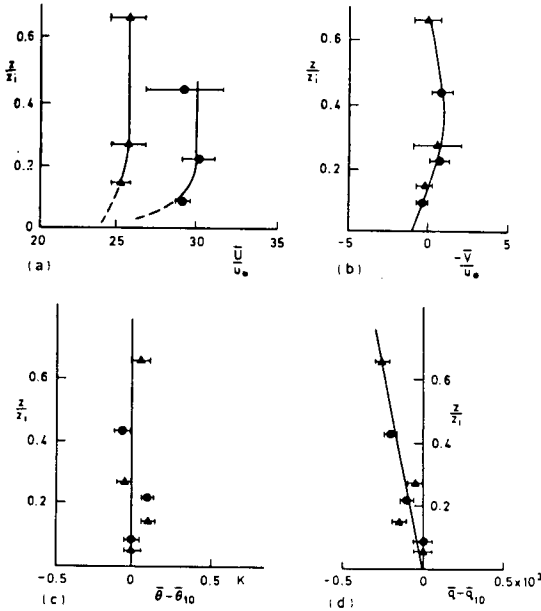
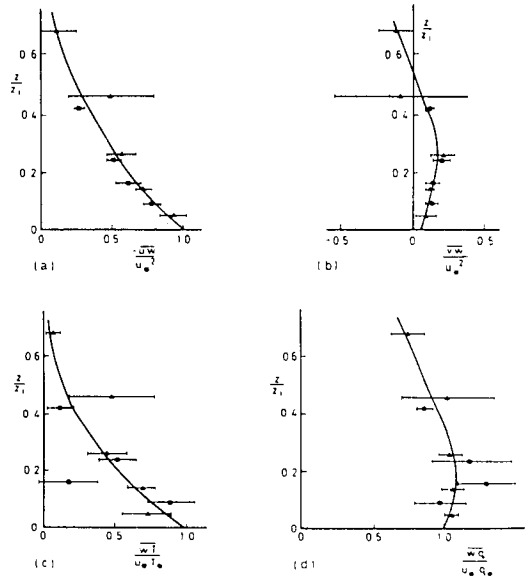


Fig. 7 Non-dimensional flux profiles for (a) $-\overline{uw}/u_*^2$, (b) \overline{vw}/u_*^2 , (c) $\overline{wT'}/u_*T_*$ and (d) \overline{wq}/u_*q_* in near-neutral conditions. T' is the fluctuating temperature ($T' \cong \theta$). Notation for stability classes is the same as in Fig. 7 (after Nicholls and Readings (1979)).



the influence of a dry-air inversion aloft which serves as a source for sensible heat and a sink for moisture. Similar results were found by Donelan and Miyake (1973) and Pennell and LeMone (1974).

Figure 7 shows the flux profiles measured by Nicholls and Readings (1979). Both stability classes give the same shape for the profiles. The fluxes \overline{uw} and $\overline{wT'}$ decrease monotonically with height in Fig. 7 whereas \overline{vw} and \overline{wq} have maxima near 0.2 h. Although the measurements have been limited to the region below the entrainment layer, the shape of the temperature flux profile is consistent with negative values in the entrainment layer. Extrapolation of the humidity flux profile to the top of the ABL gives positive values. These results are in agreement with the measurements of Pennell and LeMone (1974) who measured the profiles up to the top of the ABL under fair weather conditions (with cloudbands) ($-h/L = 1.5$) and found negative temperature fluxes and positive humidity fluxes in the entrainment region.

Profiles of the standard deviations of u, v, w, θ and q were also measured by Nicholls and Readings (1979) (not shown). The data for each stability class, when scaled, collapse into distinct lines; however there is a strong dependence on stability for these variables. The σ_w/u_* profile shows a maximum at $\sim 0.1 h$ for the near-neutral data ($-h/L = 0.9$). For the slightly instability data ($-h/L = 3.9$), the maximum is higher (at $\sim 0.5 h$) and more pronounced. The horizontal components also show strong variations with stability. Near neutral $\sigma_u/u_* > \sigma_v/u_*$ especially near the surface, but for the slightly unstable class the two components are approximately equal. The equation for σ_u and σ_v in the surface layer, proposed by Panofsky et al. (1977):

$$\sigma_u/u_* = \sigma_v/u_* = (12 - 0.5 h/L)^{1/3} \dots 41$$

describes the behaviour of the slightly unstable class, but not the near-neutral case. The standard deviation for temperature and humidity are similar to one another and show strong dependence on stability.

The equation describing the budget of turbulent kinetic energy in steady, horizontally homogeneous conditions can be written as:

$$\frac{\tau}{\rho} \frac{\partial V}{\partial z} + \frac{g}{T_v} \overline{wT'_v} - \frac{\partial}{\partial z} \overline{we} - \varepsilon = R \quad \dots 42$$

where the first term represents the shear production, the second the buoyancy production, the third the divergence of the vertical transport of turbulent kinetic energy e , the fourth the dissipation and the term on the right is the residual term (mainly the divergence of the pressure-velocity covariance but would also include measurement errors). The profiles of each of the above terms have been measured by Pennell and LeMone (1974) (not shown). They compare the measurements to the model predictions of Lenschow (1974), which was developed for convective conditions where the shear term is insignificant. For near-neutral upper layer, however, the shear term is important and Pennell and LeMone use the measured shear term in their comparison. The agreement between the observations and the model is very good, although it is not completely definitive because the observed shear was used in the model.

Mixed-layer scaling

As the stability parameter $-h/L$ becomes large, convective motions in the region above the surface layer ($z/h > 0.1$) act to destroy the gradients of mean quantities and produce nearly uniform profiles of U , V and Θ . This layer is known as the mixed layer. Usually the profile of Q is less uniform with height than Θ , because of entrainment of drier air at the top of the ABL. Figure 8 shows the profiles of mean wind, geostrophic wind, potential temperature and specific humidity for 1500 local time of Day 33 of the Wangara Experiment ($-h/L \approx 120$).

The scales for velocity, temperature and humidity in this layer are:

$$w_* \equiv ((gh/\Theta_v) \overline{w\theta'_{0v}})^{1/3}, \quad \Theta_{*v} \equiv \overline{w\theta'_{0v}}/w_*, \quad \text{and} \quad Q_* \equiv \overline{wq'_{0v}}/w_*. \quad \dots 43$$

In Fig. 9 we show non-dimensional profiles of virtual potential temperature and specific humidity for five days of measurements in a maritime convective boundary layer, 70 km east of Townsville (Hartmann 1990) ($5.5 \leq -h/L \leq 15.2$, average $-h/L = 10.0$). The slope of $\Theta_v/\Theta_{*v} \approx 0$ and $Q/Q_* \approx -6$ throughout most of the mixed layer is consistent with the results of AMTEX (Wyngaard et al. 1978).

The non-dimensional gradient of the mean value of any passive scalar variable C in the mixed layer can be written as the sum of two functions,

Fig. 8 Mean profiles of wind components, geostrophic wind components, potential temperature and specific humidity at 1500 local time, Day 33 of the Wangara Experiment. The heights of the convective boundary layer z_i (or in our notation h) and the transition layer are indicated (after Deardorff (1978)).

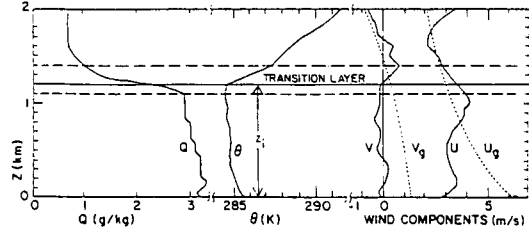
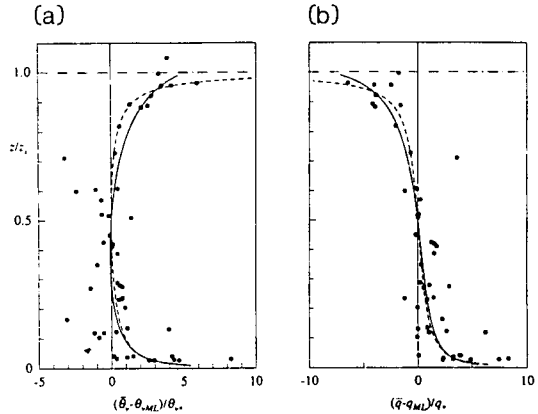


Fig. 9 Non-dimensional profiles of (a) virtual potential temperature and (b) specific humidity for data taken in conditions during the Evaporation from the Coral Sea (ECOS) Experiment. The dashed lines are for best fits to the top-down, bottom-up profile formula of Moeng and Wyngaard (1984) and the solid lines are for that of Sorbjan (1989) (after Hartmann (1990)).



one (g_t) representing top-down diffusion (driven by entrainment processes at the top of the ABL) and the other (g_b) bottom-up diffusion (driven by surface forcing):

$$(h/c_*) \partial C/\partial z = g_b(z/h) + g_t(z/h) \quad \dots 44$$

where c_* is the mixed-layer scale for C . Moeng and Wyngaard (1984) and Sorbjan (1989, pp. 102–121) derive asymmetrical expressions for g_b and g_t . As seen in Fig. 9 the data give good agreement with the integral of Eqn 44, using the expressions of Moeng and Wyngaard, and Sorbjan. The diffusivities for Θ_v and Q are nearly equal in bottom-

up diffusion and are larger than their respective values for top-down diffusion. Also the magnitude of the diffusivity for Q is nearly four times larger than the one for Θ_v for top-down diffusion, indicating that moisture is transferred much more efficiently than buoyancy in this process.

Figure 10 shows the non-dimensional profiles for the heat and moisture fluxes (Hartmann 1990). The heat flux (Fig. 10(a)) decreases linearly with height and becomes negative at $z = 0.75$ h. The ratio of the interfacial heat flux (at $z = h$) to the surface value is -0.33 in these measurements. The profile of the buoyancy flux (g/Θ_v) $\overline{w\theta}_v$ exhibits similar behaviour, decreasing linearly with height, becoming negative at $z = 0.86$ and having an interfacial to surface ratio of -0.165 . However, the measurements for the moisture flux (Fig. 10(b)) do not obey mixed-layer scaling, i.e. they do not collapse onto a single curve (also see LeMone 1980; Druilhet et al. 1983). The upper part of the profile is dominated by entrainment dynamics, rather than the surface flux. The top-down moisture flux \overline{wq}_t can be defined by subtracting the bottom-up flux from the total flux:

$$\overline{wq}_t = \overline{wq} - \overline{wq}_0 (1 - z/h) \quad \dots 45$$

The appropriate scales for the top-down moisture flux are w_* and q_{**} where

$$q_{**} \equiv \overline{wq}_t / w_* \quad \dots 46$$

and \overline{wq}_i is the interfacial moisture flux. A plot of the non-dimensional profile of \overline{wq}_i is given in Fig. 11. Although the measurements still show appreciable scatter, a linear profile emerges. Other studies (e.g. some profiles from LeMone 1980; Wayland and Raman 1989; Chou and Ferguson 1991) measure \overline{wq} profiles that do obey mixed-layer scaling and decrease linearly with height in a similar way to the $\overline{w\theta}_v$ profile, but remain positive at all heights $z \leq h$.

Fig. 10 Non-dimensional profiles of (a) heat flux and (b) moisture flux for the ECOS data, using mixed-layer scaling (after Hartmann (1990)).

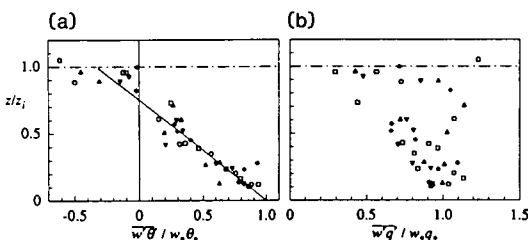
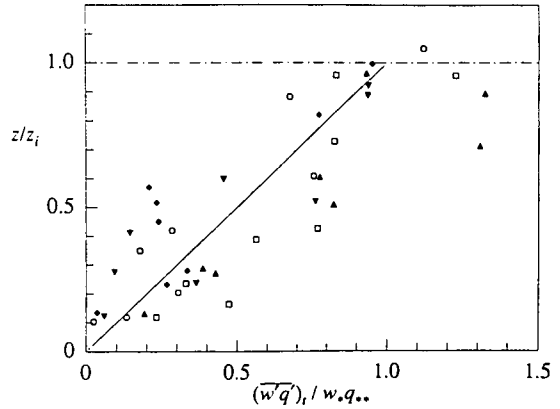


Fig. 11 Non-dimensional profile of top-down moisture flux for the ECOS data, using interfacial scaling (after Hartmann (1990)). The line represents $\overline{wq} = z/h$.



The measurements so far have included the contributions of low frequency, large eddies. In large eddy simulation (LES) models the grid spacing is about 50 to 100 m. Below this limit the turbulent transport processes must be parameterised. Figure 12 shows non-dimensional profiles of $\overline{w\theta}_v$, $w\theta$ and \overline{wq} computed from high-pass filtered data with a cut-off wavelength of 0.1 h (Hartmann 1990). In each case the data collapse to a single curve and remain positive at all heights, indicating that the entrainment dynamics (negative fluxes and top-down diffusion of \overline{wq}) is a low frequency phenomenon. Some LES models, on the other hand, have a tendency to produce negative subgrid-scale heat fluxes near the inversion (e.g. Moeng 1984; Schmidt and Schumann 1989) which indicates a defect in their subgrid-scale parameterisation.

In Figs 13 to 15 we present atmospheric data (Caughey and Palmer 1979; Lenschow et al. 1980; Druilhet et al. 1983; and Hartmann 1990) and laboratory data (Adrian et al. 1986; Deardorff and Willis 1985; Kumar and Adrian 1986) for variances of vertical velocity, potential temperature and moisture in the mixed layer. The solid line indicates the free convection-layer prediction:

$$\overline{w^2} / w_*^2 = 1.8 (z/h)^{2/3} \quad \dots 47$$

The measurements in Fig. 13 show significant deviations from this curve by $z = 0.1$ h. This expression was modified by Lenschow et al. (1980) to fit the AMTEX data by making the right-hand side of Eqn 47 equal to $1.8 (z/h)^{2/3} (1 - 0.8 z/h)^2$. The laboratory data agree well with the atmospheric data up to $z \approx 0.75$ h, but above that height

Fig. 12 Non-dimensional profiles of (a) buoyancy flux, (b) heat flux and (c) moisture flux in convective conditions computed from ECOS data treated with high-pass filters with a cut-off wavelength of 0.1 h (after Hartmann (1990)).

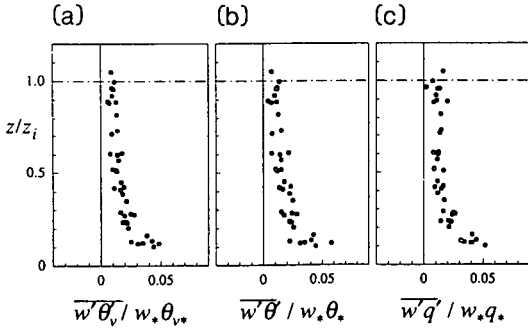
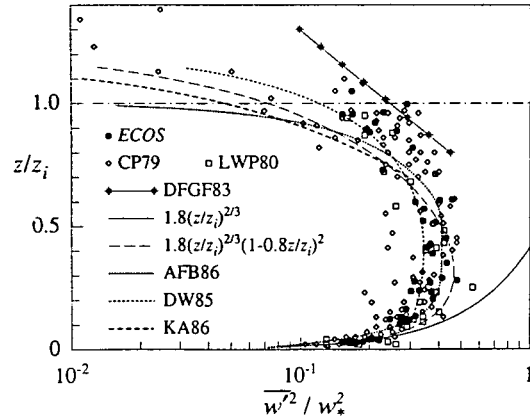
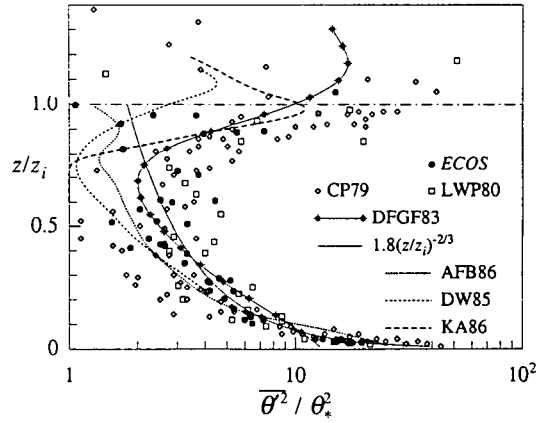


Fig. 13 Non-dimensional profile of vertical velocity variance from ECOS data in convective conditions compared with laboratory and atmospheric data. CP79 refers to the Minnesota/Ashchurch data (Caughey and Palmer 1979), LWP80 to the AMTEX data (Lenschow et al. 1980) and DFGF83 to aircraft data over France (Druihlet et al. 1983). The thick dashed lines refer to laboratory experiments: AFB86: Adrian et al. (1986); DW85: Deardorff and Willis (1985); KA86: Kumar and Adrian (1986) (after Hartmann 1990).



tend to exhibit smaller variances. The entrainment dynamics (including gravity wave-turbulence interaction) may be different for the two cases (the laboratory experiments have no mean wind shear nor clouds). Also the strength of the capping inversion may differ in the two cases. Other data sources (not shown) are eastern Color-

Fig. 14 The same as Fig. 13, except for non-dimensional potential temperature variance (after Hartmann (1990)).



ado (Lenschow 1974), Moree, NSW (Coulman 1978), METROMEX (Hildebrand and Ackerman 1984), Phoenix 78 (Young 1988b), GATE (LeMone 1980) and the laboratory data of Willis and Deardorff (1974) and Hibberd (1990).

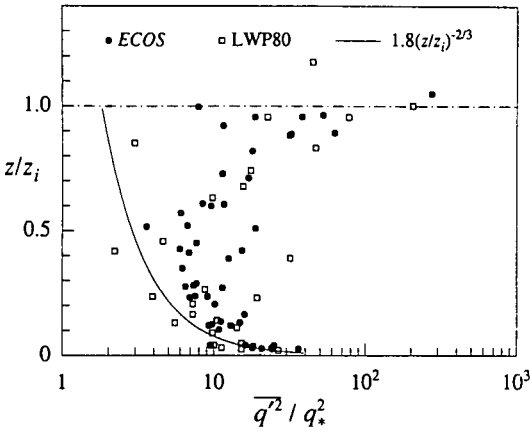
In Fig. 14 the free convection prediction for the potential temperature variance holds up to $z \approx 0.6$ h. Again the laboratory data give smaller variances than the field data near the top of the profile. The free convection prediction for humidity variance (Fig. 15) does not agree with the data above $z \approx 0.1$ h. In this case there are no laboratory data for comparison. The shape of the profile is similar to the potential temperature variance profile; both profiles show considerable scatter near the top.

These statistics and others, such as $\overline{\theta q}$, $\overline{w^3}$, $\overline{\theta v^3}$, $\overline{w\theta^2}$ and $\overline{w^2\theta v}$, in the mixed layer can be decomposed into top-down and bottom-up components and scaled with local variables to give a description of the entire profile (Sorbjan 1989, 102-21; Hartmann 1990).

The turbulent energy budget for convective conditions (with stratocumulus cloud and strong cold air advection) ($-h/L \approx 32$) was measured during the AMTEX Experiment by Lenschow et al. (1980) (not shown). Again the pressure-velocity correlation term was not measured. The magnitude of the shear term decreases rapidly with height. The sum of the buoyancy and transport terms is balanced by the dissipation term throughout most of the ABL. Their residual term is small.

Recently there has been much interest in the organised, coherent structures which form in the convective boundary layer. These include rolls and cloud streets (when some wind shear is still

Fig. 15 The same as Fig. 13, except for non-dimensional specific humidity variance (after Hartmann (1990)). Note only the AMTEX data are available for comparison.



present, typically $3 < -h/L < 30$) (Hein and Brown 1988; Wayland and Raman 1989; Martin and Bakan 1991; Chou and Ferguson 1991; Smedman 1991), and more convective structures (typically $-h/L > 50$) such as thermals (Hunt et al. 1988; Young 1988a,c,d; Williams and Hacker 1992), downdrafts (Spillane and Hess 1988), convection patterns formed by updraft convergence lines (Webb 1977, 1984; Kropfli and Hildebrand 1980; Williams 1991), hexagonal mesoscale convective cells (Hsu and Sun 1991) and shallow convection vortices/dust devils (Hess et al. 1988; Hess and Spillane 1990). Dual Dopplar radar observations (Kropfli and Hildebrand 1980) are able to detect convergence lines of updrafts between areas of downdrafts; these lines form the 'walls' of convection cells and have a height of ≈ 0.1 h. At the top of the mixed layer convective updrafts penetrate into the stable layer above creating domes. The presence of substantial wind shear above the mixed layer, such as might occur near coastlines or over hills, can lead to the occurrence of Kelvin-Helmholtz instability in the transition zone (Deardorff 1978).

Local similarity in stable conditions

Nieuwstadt (1984, 1985), Sorbjan (1989) and Derbyshire (1990) have extended similarity theory to the upper part of the stable boundary layer by replacing the surface turbulence scales u_* , T_* and q_* with local values:

$$\begin{aligned} \mathcal{U}_* &\equiv (\tau(z)/\rho)^{1/2}, \quad \mathcal{T}_{*v} \equiv -\overline{w\theta_v}(z)/\mathcal{U}_* \\ \text{and } \mathcal{Q}_* &\equiv -\overline{wq}(z)/\mathcal{U}_* \end{aligned} \quad \dots 48$$

Immediately above the surface layer the non-dimensional gradients, for example, can be written as:

$$\begin{aligned} (kz/\mathcal{U}_*) \partial(U^2 + V^2)^{1/2}/\partial z &= F_u(z/\Lambda), \\ (kz/\mathcal{T}_{*v}) \partial\Theta_v/\partial z &= F_\theta(z/\Lambda) \\ \text{and } (kz/\mathcal{Q}_*) \partial Q/\partial z &= F_q(z/\Lambda) \end{aligned} \quad \dots 49$$

As z/Λ increases the flow eventually becomes stable enough so that z is no longer an important parameter (at $z/\Lambda \approx 1$), and non-dimensional quantities should approach constant values; for example:

$$\begin{aligned} (k\Lambda/\mathcal{U}_*) \partial(U^2 + V^2)^{1/2}/\partial z &= A_u, \\ (k\Lambda/\mathcal{T}_{*v}) \partial\Theta_v/\partial z &= A_\theta \\ \text{and } (k\Lambda/\mathcal{Q}_*) \partial Q/\partial z &= A_q \end{aligned} \quad \dots 50$$

Near the ground where $\Lambda \approx L$ integration of Eqn 50 gives linear profiles which have been observed by Hicks (1976) and Kondo et al. (1978).

Under these conditions the variances become

$$\begin{aligned} \sigma_i^2(z)/\mathcal{U}_*^2 &= C_i, \quad e(z)/\mathcal{U}_*^2 = C_e \text{ and} \\ \sigma_{\theta_v}^2(z)/\mathcal{T}_{*v}^2 &= C_{\theta_v} \end{aligned} \quad \dots 51$$

where $i = u, v$ or w and the C_s are constants.

Nieuwstadt (1984, 1985) has demonstrated this scaling for Cabauw tower data and Sorbjan (1989) for the Minnesota tethered balloon data. Here we present the aircraft data of Lenschow et al. (1988a,b) for the SESAME Experiment in central Oklahoma. The data were collected during constant-level flights over grass-covered rolling hills a few tens of metres high. The flights were in the early evening or early morning and the average stability for the four flights was $h/L = 1.6$.

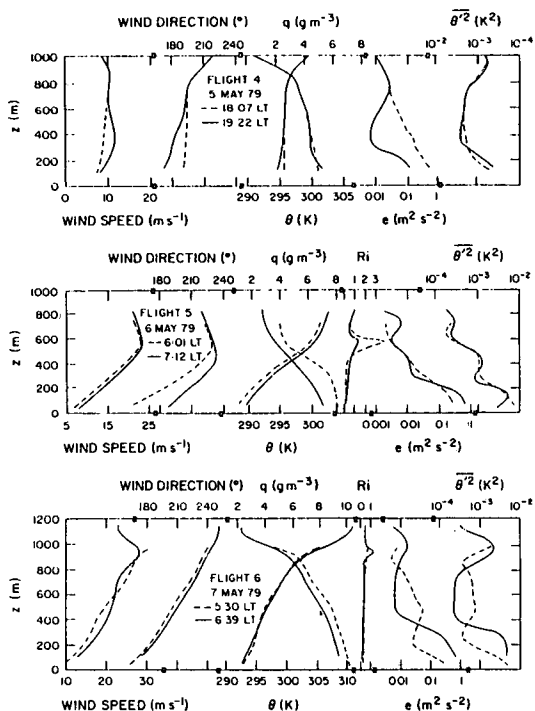
Figure 16 shows the profiles for the mean wind speed and direction, potential temperature, Richardson number, turbulent kinetic energy and temperature variance for Flights 4, 5 and 6. Flights 5 and 6 show very strong nocturnal supergeostrophic jets (130 per cent and 50 per cent greater than geostrophic, respectively) due to terrain slope effects and the diurnal variations in eddy stress and buoyancy forces.

The height of the stable boundary layer h is more difficult to determine than in the convective case. Lenschow et al. define h as the height where e drops to five per cent of its near-surface value (200, 300 and 400 m, respectively, for Flights 4, 5 and 6). Zilitinkevich (1972) proposes that in steady, equilibrium conditions h is given by:

$$h|f|/u_* = d (u_*|f|L)^{-1/2} \quad \dots 52$$

where f is the Coriolis parameter and d a universal constant. In practice d decreases with time after sunset. Lenschow et al. find an average d for four flights of 0.37 which is consistent with previous observations (Caughey et al. 1979; Garratt 1982), but there is considerable scatter. Based on a nu-

Fig. 16 Profiles of the mean wind speed and direction, potential temperature, Richardson number (for Flights 5 and 6), turbulent kinetic energy and temperature variance for Flights 4, 5 and 6 in stable conditions with continuous turbulence (after Lenschow et al. (1988a)).



merical study Estouiral and Guedalia (1990) develop a parametrisation for d' in the simpler relation $h|f|/u_* = d'$.

The shapes of the profiles of stress and heat flux in stable conditions have been predicted by simple analytical models based on constant flux Richardson number (Nieuwstadt 1984, 1985; Sorbjan 1989; Lenschow et al. 1988a; Derbyshire 1990). They find:

$$\tau(z)/\rho = u_*^2 (1 - z/h)^{\alpha_1} \quad \dots 53$$

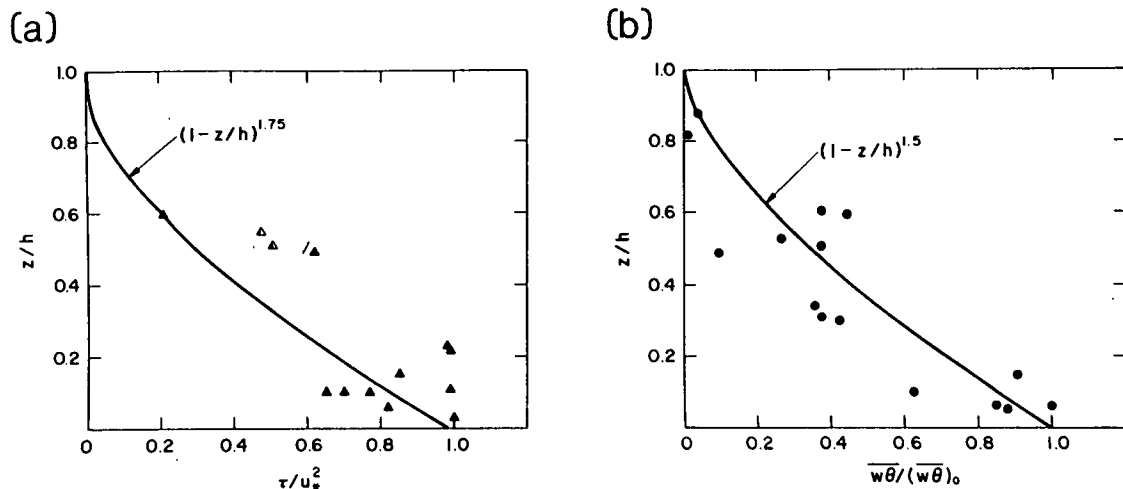
$$\overline{w\theta} = \overline{w\theta}_0 (1 - z/h)^{\alpha_2} \quad \dots 54$$

Unfortunately these are not similarity expressions and α_1 and α_2 are not universal constants, but depend on the time after sunset, baroclinicity, slope of terrain, etc. (Sorbjan 1989). Lenschow et al. find $\alpha_1 = 1.75$ and $\alpha_2 = 1.5$; Nieuwstadt (1984) finds $\alpha_1 = 1.5$ and $\alpha_2 = 1.0$ for the Cabauw data in quasi-steady conditions several hours after the transition; Sorbjan (1989) finds $\alpha_1 = 2$ and $\alpha_2 = 3$ for the strongly evolving transition period of the Minnesota data. Figure 17 shows the data of Lenschow et al. for the momentum and heat flux profiles. The data agree with the predicted relations, but the large scatter doesn't rule out other exponents.

If Eqns 53 and 54 are combined with Eqn 51 then the variances can be determined as a function of height. For example, variances normalised by the square of the surface friction are predicted to follow the relation $\sim (1 - z/h)^{1.75}$.

Lenschow et al. (1988a) also measured profiles of the terms in the turbulent energy budget. Again the pressure-velocity correlation term was not measured. In this stability regime the budget is

Fig. 17 Profiles of (a) momentum flux and (b) heat flux normalised by the values at the lowest flight levels in stable conditions with continuous turbulence (after Lenschow et al. (1988a)).

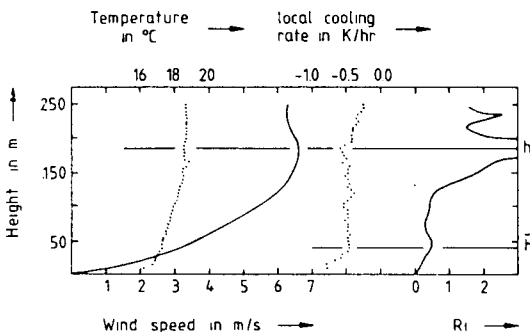


mainly a balance between shear production and turbulent energy dissipation, however they found a significant residual in their measurements.

Stable intermittent layer

As $h/L \rightarrow \infty$ the turbulence becomes intermittent. Wittich (1991) has studied the stable intermittent layer using data from a 300 m tower near

Fig. 18 Profiles of mean wind speed, temperature, local cooling rate and Richardson number in stable conditions with intermittent turbulence. The depth of the surface inversion layer h and the nocturnal boundary layer h are indicated (after Wittich (1991)).

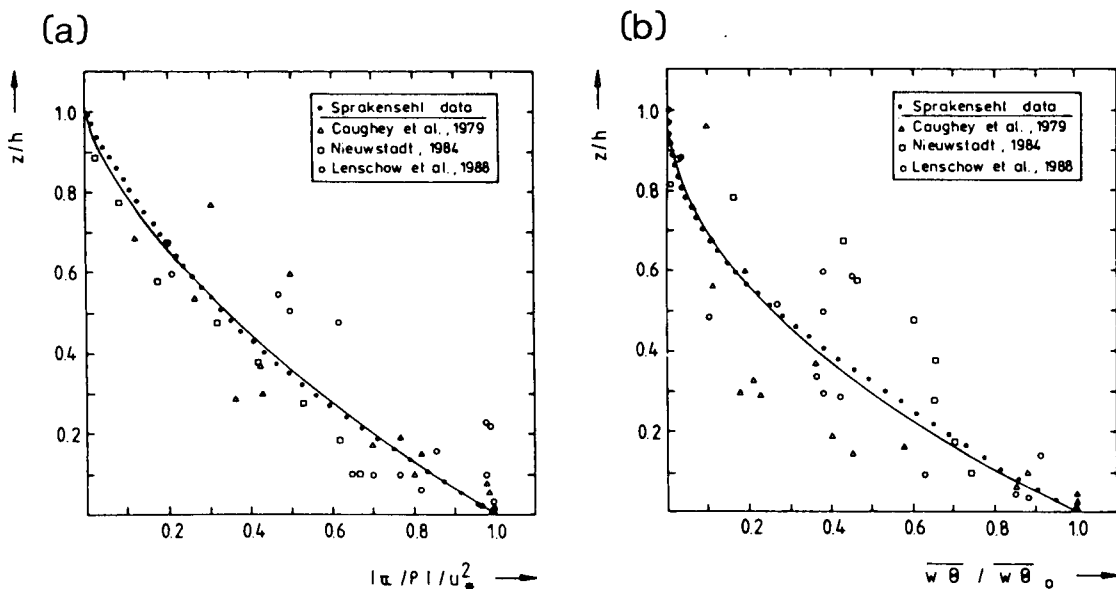


Sprakensehl, northern Germany. Turbulent fluxes were not directly measured but were determined by integration of the geostrophic departure and thermal energy equations.

The vertical profiles of mean wind speed and temperature, local cooling rate and Richardson number are shown in Fig. 18 for a clear night with $h/L \approx 17$. The height of the surface inversion layer is ≈ 40 m and $h \approx 185$ m. The various terms contributing to the local cooling rate were also measured (not shown). The turbulent heat flux and the advection terms dominate the balance throughout most of the boundary layer. Near the top of the boundary layer $0.8 < z/h < 1$ radiational cooling is greater than turbulent cooling.

A comparison of the Sprakensehl data with other observations of non-dimensional momentum and heat flux profiles is given in Fig. 19. All of the profiles have the same general shape. The Sprakensehl data give $\alpha_1 = 2$ and $\alpha_2 = 1.5$. The lack of scatter evident in the Sprakensehl is a result of the amount of smoothing inherent in the integral techniques. Because of the uncertainties in obtaining reliable assessments of the geostrophic wind and in the boundary conditions, direct eddy correlation measurements of the fluxes are generally preferred. However in very stable conditions the magnitudes of the fluxes are small and direct measurement may be difficult or

Fig. 19 Non-dimensional profiles of (a) momentum flux and (b) heat flux in stable conditions with intermittent turbulence (after Wittich (1991)).



impossible; integral methods are an alternative. A similar study of the stress profile in the stable intermittent boundary layer (at Plateau Station, Antarctica) was carried out by Lettau and Dabberdt (1970), using the geostrophic departure technique.

Profiles of the variances $\overline{u^2}$, $\overline{v^2}$, $\overline{w^2}$, $\overline{\theta_v^2}$ and $\overline{q^2}$ have apparently not been well measured in the stable intermittent boundary layer. In the region $L \leq z \leq h$ internal gravity waves are usually present in these conditions (see e.g. Cheung 1991). These waves would not transport much heat or moisture, but would be responsible for variances of θ_v and q given by (Deardorff 1978):

$$\overline{\theta^2} = (1/2) (a\partial\theta/dz)^2 \quad \dots 55$$

$$\overline{q^2} = (1/2) (a\partial Q/dz)^2 \quad \dots 56$$

where a is the amplitude of the wave. For $a = 50$ m and $\partial\theta/\partial z = 1$ K/100 m, then $\overline{\theta^2}$ is $O(0.3K)$ independent of the surface fluxes.

Generalised Rossby number similarity

Above the surface layer where M-O similarity holds, Kazanski and Monin (1961) suggest that non-dimensionalised profiles of the wind components, potential temperature, and specific humidity can be expressed as universal similarity functions. We write these profiles, or 'defect laws', as:

$$\begin{aligned} (U - U_b)/u_* &= f_u(z/h_b, h_b/L), \\ (V - V_b)/u_* &= f_v(z/h_b, h_b/L), \\ (\Theta - \Theta_b)/T_* &= f_\theta(z/h_b, h_b/L) \text{ and} \\ (Q - Q_b)/q_* &= f_q(z/h_b, h_b/L) \quad \dots 57 \end{aligned}$$

where the subscript b indicates bulk or characteristic scales for the ABL. Formally Eqn 57 applies in the limit as the surface Rossby number $Ro \rightarrow \infty$, where $Ro \equiv |\underline{U}_g|/|f|z_0$, $|\underline{U}_g|$ is the geostrophic wind and f the Coriolis parameter. This means that Eqn 57 applies to the outer part of the ABL and is independent of the roughness length.

The functions in Eqn 57 could be expanded to include the effects of the ratio of the rotational height $u_*|f|$ to h_b , geostrophic wind shear (baroclinicity), non-stationarity, terrain slope, and other factors (see e.g. Sorbjan 1989; Garratt 1992). However, in a practical sense, it is often difficult or impossible to determine the functional relationships for a large number of independent parameters from field data. In the convective boundary layer if we take h_b to be h and U_b , V_b , Θ_b and Q_b to be the mixed-layer averaged values, then there is evidence that the additional vari-

ables probably play a minor role (Brutsaert and Sugita 1991; Garratt 1992). However, in stable conditions the shapes of the profiles of momentum and heat flux are dependent on the time after sunset, baroclinicity, terrain slope, etc. (see Eqns 53 and 54), indicating that under these conditions the form of Eqn 57 may be incomplete for general application.

In the limits as $z/h \rightarrow 0$ and $z/z_0 \rightarrow \infty$, it is assumed that there is a region of overlap where Eqns 14 to 16 and Eqn 57 are simultaneously valid. Matching these expressions yields a set of equations known as the resistance laws:

$$\ln(h_b/z_0) - kV_b/u_* = A(h_b/L) \quad \dots 58$$

$$-kV_b/u_* = B(h_b/L) \text{ sign}(f) \quad \dots 59$$

$$\ln(h_b/z_H) + k(\Theta_b - \Theta_0)/T_* = -C(h_b/L) \quad \dots 60$$

$$\ln(h_b/z_Q) + k(Q_b - Q_0)/q_* = -D(h_b/L) \quad \dots 61$$

where the stability functions A , B , C and D ultimately must be determined by experiment. Once A , B , C and D are known then Eqns 58 to 61 can be used to evaluate the surface fluxes. (It should be noted that some authors reverse the definitions of A and B in Eqns 58 and 59.)

Recently Zilitinkevich (1989) and Byun (1991), following an approach suggested by Long (1974), have extended the logarithmic profiles of Eqns 14 to 16 in height by adding polynomial or power law terms. The coefficients of these terms are evaluated by imposing boundary conditions. These functions are then matched with Eqn 57 and relations for the functional forms of A , B , and C are derived. Derbyshire (1990) has used the model of Nieuwstadt (1984, 1985) to determine A and B in stable conditions. Summaries of various authors' prescriptions for A , B and C based on models and observations, including laboratory data, are given by Zilitinkevich (1989) and Byun (1991). Most of the predictions fall within the scatter of the data, which is large near neutral and on the stable side. To date there has been little work done on determining the moisture function D (see Brutsaert 1982, p. 85). Recent extensions of the theory to non-homogeneous terrain are discussed by Brutsaert and Sugita (1991) and Emeis and Zilitinkevich (1991) and an application of determining ocean winds for marine modelling is given by McIntosh and Hubbert (1992).

Surface inhomogeneities

Clarke and Hess (1974) recognised the importance of surface inhomogeneities even at reasonably homogeneous sites such as at the Wangara Experiment. Recently this problem has received renewed attention because of its importance to parametrising subgrid-scale transport processes

in numerical modelling. At a height l_b , called the blending height, internal boundary layers created by different isolated obstacles or areas of roughness merge and effective surface properties, e.g. the effective surface roughness for momentum z_{0eff} , can be defined (Wieringa 1986; Mason 1988; Claussen 1989, 1990, 1991):

$$(l_b/L_h) \ln^2(l_b/z_{0eff}) = 2k^2 \quad \dots 62$$

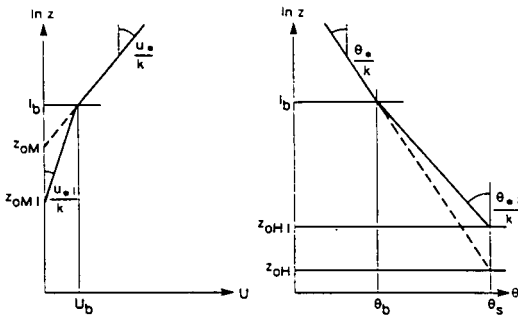
where L_h is the horizontal length scale of the roughness variations. An alternative relation for z_{0eff} , based on a different estimate of the gradient of the perturbation velocity, is given by (Claussen 1988, 1990; Beljaars and Taylor 1989; Beljaars and Holtslag 1991; Wood and Mason 1991):

$$(l_d/L_h) \ln(l_d/z_{0eff}) = ck \quad \dots 63$$

where c is a constant (Claussen (1991) recommends $c \approx 1.75$). Sometimes l_d is called the diffusion height ($l_d > l_b$), but sometimes l_d is called the blending height and is denoted by l_b . In Fig. 20 we illustrate the effect of a heterogeneous surface on the profiles of wind speed and temperature. Below l_b the profiles are in equilibrium with the local surface properties (indicated by the subscript 1), but above l_b the profiles are in equilibrium with the areally averaged properties. The differences between local and areally averaged values produces kinks in the profiles and different extrapolated roughness lengths depending on where in the profile the extrapolation begins. Assuming constant heat flux with height and logarithmic profiles a simple estimate of the effective temperature roughness length can be obtained (Beljaars and Holtslag 1991):

$$\ln(l_b/z_{Heff}) = \ln(l_b/z_{01}) \ln(l_b/z_{H1}) / \ln(l_b/z_{0eff}) \quad \dots 64$$

Fig. 20 Schematic diagram of near-neutral wind and potential temperature profiles for terrain with sparsely distributed obstacles that contribute significantly to the areally-averaged surface drag. l_b is the blending height. The subscript 1 indicates local values (after Beljaars and Holtslag (1991)).



For $l_b \approx 20$ m, and the ratio of local roughness lengths $z_{01}/z_{H1} \approx 10$, then Eqn 64 leads to a ratio of areally averaged roughness lengths $z_{0eff}/z_{Heff} = O(10^4)$ when z_{0eff} is about an order of magnitude larger than z_{01} . Extension of the theory to non-neutral cases has been studied by Wood and Mason (1991), Grant (1991) and Claussen (1991). The effective roughness length for momentum can be estimated from a weighted average relation:

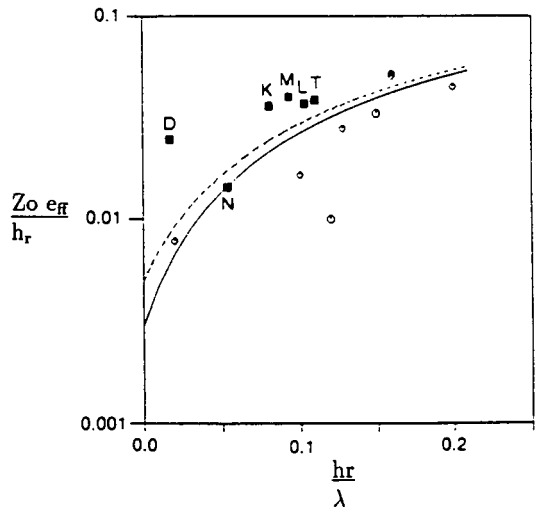
$$(1/\ln^2(l_b/z_{0eff})) = \sum_i (f_i/\ln^2(l_b/z_{0i})) \quad \dots 65$$

where f_i is the fractional cover of local roughness length z_{0i} .

Terrain also can play a significant role in determining surface roughness. Recently Grant and Mason (1990) parametrised the total drag by a sum of the shear stress contribution associated with the small-scale roughness elements and form drag created by the terrain:

$$\ln^2(h_r/2z_{0eff}) = k^2/(0.5 D h_r/\lambda + k^2/\ln^2(h_r/2z_{01})) \quad \dots 66$$

Fig. 21 The variation of z_{0eff}/h_r as a function of h_r/λ . The open symbols are the results from a second-moment closure model for flow over sinusoidal orography with $z_{01} = 0.1$ and 0.3 m. The filled symbols are experimental values for (T) Thompson (1978); (N) Noihan et al. (1982); (K) Kustas and Brutsaert (1986); (M) Mason (1987); (D) Durand et al. (1987) and (L) present study. The dashed curve represents Eqn 66 for $z_{01} = 0.5$ m and $h_r = 300$ m and the solid curve for $z_{01} = 0.3$ m and $h_r = 300$ m (after Grant and Mason (1990)).



where for separated flows over sinusoidal orography $D \approx 0.3$, h_r is the height of the obstacles (trough to peak from a ridge-valley system), and λ the horizontal wavelength of the terrain. A comparison of the predictions from Eqn 65 with observations (Fig. 21) shows general agreement. For $h_r \approx 250$ m and $h_r/\lambda = 0.08$, $z_{0\text{eff}} \approx 9.0$ m! This value of $z_{0\text{eff}}$ assumes that the terrain is statistically homogeneous over an area of $O(100 \text{ km}^2)$.

Future work

In this review we have touched upon some of the recent advances in our understanding of observations and scaling of the ABL. However there are many areas in which our knowledge is incomplete. Some of these areas are mentioned below:

- There is still no definitive set of experiments determining the fundamental constants of turbulence theory, e.g. von Kármán's constant, Kolmogorov constant, neutral Prandtl number, neutral Schmidt number, the profile constants, etc. The von Kármán constant is related to the Kolmogorov constant and both should be determined in the same experiment by independent means. Are these numbers really constant or do they depend on unknown variables? A definitive set of experiments would have to measure all of the terms in the turbulent kinetic energy equation, including the pressure-velocity correlation term. (Also see the review and discussion by Frenzen and Vogel (1992) that has just appeared.)
- A careful experimental study of free convection and the mean profile relations at large instability ($-z/L > 2$) is still needed.
- The interplay between observation, theory and modelling is vital. In the stable ABL a general framework for a theory is beginning to emerge from the work of Nieuwstadt (1984, 1985), Sorbjan (1989), Lenschow et al. (1988), and Derbyshire (1990). Preliminary large-eddy simulations of the stable layer have recently been completed (Mason and Derbyshire 1990). However, the stable boundary layer will continue to be a great challenge because of the importance of terrain slope effects and drainage flow, the presence of internal gravity waves, radiation, baroclinicity, intermittency and unsteadiness. Can parametrisation of the stable intermittent boundary layer help us to parametrise clear-air turbulence for use in forecast models?
- The problems of cloud-topped ABLs and fog have not been discussed in this review, yet they are areas of great importance. These involve the interaction of turbulence and radiation. This interaction is delicately balanced for fog. A simple parametrisation of the height of the cloud-topped boundary layer would be helpful.

- Significant progress has been made in understanding the dry convective boundary layer, but the parametrisation of moist convection in the ABL needs to be better understood.
- The effect of inhomogeneities in surface properties is another area of active research. How complex does the specification of land-surface interaction need to be?
- Most measurements of bulk transfer coefficients over the sea have been performed at moderate wind speeds. More measurements of the fluxes and transfer coefficients at both low and high wind speeds are needed.
- The interaction between turbulence and gravity waves at the top of the ABL can have significant impact on the turbulent statistics in the entrainment region, especially moisture. More study of entrainment dynamics is needed. What is the height of the mixed layer when penetrative convection from below and entrainment from above create a highly convoluted surface?

The standards of research that Reg Clarke set in his ABL experiments and his insatiable curiosity and desire to understand how the atmosphere works continue to provide us with a challenging role model to follow.

Acknowledgments

It is a pleasure to acknowledge the help of Drs Anton Beljaars, Frank Bradley, Chris Fairall, John Garratt, Jörg Hacker and Mark Hibberd in preparing this review.

References

- Adrian, R.J., Ferreira, R.T.D.S. and Boberg, T. 1986. Turbulent thermal convection in wide horizontal fluid layers. *Exp. Fluids*, 4, 121–41.
- André, J.-C., Bougeault, P. and Goutorbe, J.-P. 1990. Regional estimates of heat and evaporation fluxes over non-homogeneous terrain. Examples from the HAPEX-MOBILHY programme. *Bound. Lay. Met.*, 50, 77–108.
- Arya, S.P. 1988. *Introduction to Micrometeorology*. Academic Press, New York, 307 pp.
- Beljaars, A.C.M. and Holtslag, A.A.M. 1991. Flux parametrisation over land surfaces for atmospheric models. *Jnl appl. Met.*, 30, 327–41.
- Beljaars, A.C.M. and Taylor, P.A. 1989. On the inner-layer scale height of boundary-layer flow over low hills. *Bound. Lay. Met.*, 49, 433–8.
- Betts, A.K., Desjardins, R.L., MacPherson, J.I. and Kelly, R.D. 1990. Boundary-layer heat and moisture budgets from FIFE. *Bound. Lay. Met.*, 50, 109–37.
- Blackadar, A.K. 1979. High-resolution models of the planetary boundary layer. In *Advances in Environmental Science and Engineering*, 1, 50–85.
- Bradley, E.F., Coppin, P.A. and Godfrey, J.S. 1991. Measurements of sensible and latent heat flux in the western equatorial Pacific Ocean. *J. geophys. Res.*, 96, 3375–89.
- Brutsaert, W.H. 1982. *Evaporation into the Atmosphere*. Reidel, Dordrecht, 299 pp.

- Brutsaert, W. and Sugita, M. 1991. A bulk similarity approach in the atmospheric boundary layer using radiometric skin temperature to determine regional surface fluxes. *Bound. Lay. Met.*, 55, 1–23.
- Businger, J.A. 1973. A note on free convection. *Bound. Lay. Met.*, 4, 323–6.
- Businger, J.A. 1985. The marine boundary layer, from air-sea interface to inversion. *NCAR Tech. Note*, NCAR/TN-252+STR, National Center for Atmospheric Research, Boulder, CO, 84 pp.
- Businger, J.A., Wyngaard, J.C., Izumi, Y. and Bradley, E.F. 1971. Flux profile relationships in the atmospheric surface layer. *J. Atmos. Sci.*, 28, 181–9.
- Byun, D.W. 1990. On the analytical solutions of flux-profile relationships for the atmospheric surface layer. *Jnl appl. Met.*, 29, 652–7.
- Byun, D.W. 1991. Determination of similarity functions of the resistance laws for the planetary boundary layer using surface-layer similarity functions. *Bound. Lay. Met.*, 57, 17–48.
- Carl, D.M., Tarbell, T.C. and Panofsky, H.A. 1973. Profiles of wind and temperature from towers over homogeneous terrain. *J. Atmos. Sci.*, 30, 788–94.
- Caughey, S.J. and Palmer, S.G. 1979. Some aspects of turbulence structure through the depth of the convective boundary layer. *Q. Jl R. met. Soc.*, 105, 811–27.
- Caughey, S.J., Wyngaard, J.C. and Kaimal, J.C. 1979. Turbulence in the evolving stable layer. *J. Atmos. Sci.*, 36, 1041–52.
- Charnock, H. 1955. Wind stress on a water surface. *Q. Jl R. met. Soc.*, 81, 639–40.
- Cheung, T.K. 1991. Sodar observations of the stable lower atmospheric boundary layer at Barrow, Alaska. *Bound. Lay. Met.*, 57, 251–74.
- Chou, S.-H. and Ferguson, M.P. 1991. Heat fluxes and roll circulations over the western Gulf Stream during an intense cold-air outbreak. *Bound. Lay. Met.*, 55, 255–81.
- Choudhury, B.J., Reginato, R.J. and Idso, S.B. 1986. An analysis of infrared temperature observations over wheat and calculation of latent heat flux. *Agric. For. Met.*, 37, 75–88.
- Clarke, R.H. 1970. Observational studies in the atmospheric boundary layer. *Q. Jl R. met. Soc.*, 96, 91–114.
- Clarke, R.H. 1990a. The lower atmosphere over a dry season savannah site. Part I: the observations. *Aust. Met. Mag.*, 38, 163–71.
- Clarke, R.H. 1990b. The lower atmosphere over a dry season savannah site. Part II: modelling and deductions. *Aust. Met. Mag.*, 38, 235–44.
- Clarke, R.H. 1990c. Modelling mixed-layer growth in the Koorin Experiment. *Aust. Met. Mag.*, 38, 227–34.
- Clarke, R.H. and Brook, R.R. (eds) 1979. The Koorin expedition: atmospheric boundary-layer data over tropical savannah land. *Met. Summary*, AGPS, Canberra.
- Clarke, R.H. and Hess, G.D. 1974. Geostrophic departure and the functions A and B of Rossby number similarity theory. *Bound. Lay. Met.*, 1, 267–87.
- Clarke, R.H., Dyer, A.J., Brook, R.R., Reid, D.G. and Troup, A.J. 1971. The Wangara Experiment: Boundary Layer Data. *Tech. Pap. No. 19*. CSIRO, Div. Met. Phys., Aspendale, Australia, 362 pp.
- Claussen, M. 1988. On the inner-layer scale height of boundary-layer flow over low hills. *Bound. Lay. Met.*, 44, 411–13.
- Claussen, M. 1989. Subgrid-scale fluxes and flux divergences in a neutrally stratified, horizontally inhomogeneous surface-layer. *Beitr. Phys. Atmos.*, 62, 236–45.
- Claussen, M. 1990. Area-averaging of surface fluxes in a neutrally stratified, horizontally inhomogeneous atmospheric boundary layer. *Atmos. Environ.*, 24A, 1349–60.
- Claussen, M. 1991. Estimation of areally-averaged surface fluxes. *Bound. Lay. Met.*, 54, 387–410.
- Coulman, C.E. 1978. Boundary-layer evolution and nocturnal inversion dispersal. Part II. *Bound. Lay. Met.*, 14, 493–513.
- Deardorff, J.W. 1972. Parameterisation of the planetary boundary layer for use in general circulation models. *Mon. Weath. Rev.*, 2, 93–106.
- Deardorff, J.W. 1978. Observed characteristics of the outer layer. In *Short Course on the Planetary Boundary Layer* (A.K. Blackadar (ed.)), American Meteorological Society, Boston, 101 pp.
- Deardorff, J.W. 1980. Progress in understanding entrainment at the top of a mixed layer. In *Workshop on the PBL* (J.C. Wyngaard (ed.)), American Meteorological Society, Boston, 36–66.
- Deardorff, J.W. and Willis, G.E. 1985. Further results from a laboratory model of the convective planetary layer. *Bound. Lay. Met.*, 32, 205–36.
- Delsol, F., Miyakoda, K. and Clarke, R.H. 1971. Parameterised process in the surface boundary layer of an atmospheric circulation model. *Q. Jl R. met. Soc.*, 97, 181–208.
- Derbyshire, S.H. 1990. Nieuwstadt's stable boundary layer revisited. *Q. Jl R. met. Soc.*, 116, 127–58.
- Donelan, M.A. 1990. Air-sea interaction. *The Sea: Ideas and Observations on Progress in the Study of the Seas*, Vol. 9, (B. LeMehaute and D. Hanes (eds)), Wiley-Interscience, New York, 239–92.
- Donelan, M.A. and Miyake, M. 1973. Spectra and fluxes in the boundary layer of the trade-wind zone. *J. Atmos. Sci.*, 30, 444–64.
- Driedonks, A.G.M. 1982. Models and observations of the growth of the ABL. *Bound. Lay. Met.*, 23, 283–306.
- Driedonks, A.G.M. and Dyunkerke, P.G. 1989. Current problems in the stratocumulus-topped atmospheric boundary layer. *Bound. Lay. Met.*, 47, 275–304.
- Druilhet, A., Frangi, J.P., Guedalia, D. and Fontan, J. 1983. Experimental studies of the turbulence structure parameters of the convective boundary layer. *Jnl Clim. appl. Met.*, 22, 594–608.
- Durand, P., Druilhet, A., Hedde, T. and Benech, B. 1987. Aircraft observations of the structure of the boundary layer over a rugged hilly region (MESOGERS 84 experiments). *Ann. Geophys.*, 5, Series B, 441–50.
- Dyer, A.J. 1974. A review of flux-profile relationships. *Bound. Lay. Met.*, 7, 363–72.
- Dyer, A.J. and Bradley, E.F. 1982. An alternative analysis of flux-gradient relationships at the 1976 ITCE. *Bound. Lay. Met.*, 22, 3–19.
- ECMWF. 1989. Parametrization of fluxes over land surface, Workshop Proceedings, 24–26 October 1988, ECMWF, Shinfield Park, UK, 392 pp.
- Emeis, S. and Zilitinkevich, S.S. 1991. Resistance law, effective roughness length, and deviation angle over hilly terrain. *Bound. Lay. Met.*, 55, 191–8.
- Estournel, C. and Guedalia, D. 1990. Improving the diagnostic relation for the nocturnal boundary-layer height. *Bound. Lay. Met.*, 53, 191–8.
- Frenzen, P. and Vogel, C.A. 1992. The turbulent kinetic energy budget in the atmospheric surface layer: a review and an experimental reexamination in the field. *Bound. Lay. Met.*, 60, 49–76.
- Friehe, C.A. 1987. Review of atmospheric boundary layer research, 1983–1986. *Rev. Geophys.*, 25, 387–92.
- Garratt, J.R. 1977. Review of drag coefficients over oceans and continents. *Mon. Weath. Rev.*, 105, 915–29.
- Garratt, J.R. 1980. Surface influence upon profiles in the atmospheric near-surface layer. *Q. Jl R. met. Soc.*, 106, 803–19.
- Garratt, J.R. 1982. Observations on the nocturnal boundary layer. *Bound. Lay. Met.*, 22, 21–48.
- Garratt, J.R. 1990. The internal boundary layer—A review. *Bound. Lay. Met.*, 50, 171–203.
- Garratt, J.R. 1992. *The Atmospheric Boundary Layer*. Cambridge University Press, Cambridge (in press).
- Garratt, J.R. and Hicks, B.B. 1973. Momentum, heat and water vapour transfer to and from natural and artificial surfaces. *Q. Jl R. met. Soc.*, 99, 680–7.
- Garratt, J.R. and Hicks, B.B. 1990. Micrometeorological and

- PBL experiments in Australia. *Bound. Lay. Met.*, 50, 11–29.
- Geernaert, G.L., Davidson, K.L., Larsen, S.E. and Mikkelsen, T. 1988. Wind stress measurements during the Tower Ocean Wave and Radar Dependence Experiment. *J. geophys. Res.*, 93, 13,913–23.
- Geernaert, G.L. and Plant, W.J. (eds). 1990. *Surface Waves and Fluxes*. Vol. 1 – Current Theory, 337 pp.; Vol. 2 – Remoting Sensing. Kluwer Academic Publishers. Dordrecht.
- Godfrey, J.S. and Beljaars, A.C.M. 1991. On the turbulent fluxes on buoyancy, heat and moisture at the air-sea interface at low wind speeds. *J. geophys. Res.*, 96, 22,043–8.
- Golitsyn, G.S. and Grachov, A.A. 1986. Free convection of multicomponent media and parameterisation of air-sea interaction at light winds. *Ocean Air Interact.*, 1, 57–78.
- Grant, A.L.M. 1991. Surface drag and turbulence over an inhomogeneous land surface. *Bound. Lay. Met.*, 56, 309–37.
- Grant, A.L.M. and Mason, P.J. 1990. Observations of boundary layer structure over complex terrain. *Q. Jl R. met. Soc.*, 116, 159–86.
- Hartmann, J. 1990. Airborne Turbulence Measurements in the Maritime Convective Boundary Layer. Ph.D. dissertation. School of Earth Sciences, Flinders University, Bedford Park, SA.
- Hasse, L. 1990. Oceanic micrometeorological field experiments: An historical perspective. *Bound. Lay. Met.*, 50, 139–46.
- Haugen, D.A. (ed.) 1973. *Workshop on Micrometeorology*. American Meteorological Society, Boston, 392 pp.
- Hein, P.F. and Brown, R.A. 1988. Observations of longitudinal roll vortices during Arctic cold air outbreaks over open water. *Bound. Lay. Met.*, 45, 177–99.
- Hess, G.D. and Spillane, K.T. 1990. Characteristics of dust devils in Australia. *Jnl appl. Met.*, 29, 498–507.
- Hess, G.D., Hicks, B.B. and Yamada, T. 1981. The impact of the Wangara experiment. *Bound. Lay. Met.*, 20, 135–74.
- Hess, G.D., Spillane, K.T. and Lourens, R.S. 1988. Atmospheric vortices in shallow convection. *Jnl appl. Met.*, 27, 305–17.
- Hibberd, M.F. 1990. Experimental investigations of turbulence and dispersion in a laboratory model of the planetary convective boundary layer. *SECV Research Fellowship Annual Rept.* CSIRO Div. Atmos. Res., Aspendale, 18 pp.
- Hicks, B.B. 1975. A procedure for the formulation of bulk transfer coefficients over water. *Bound. Lay. Met.*, 8, 515–24.
- Hicks, B.B. 1976. Wind profile relationships from the 'Wangara' experiment. *Q. Jl R. met. Soc.*, 102, 535–51.
- Hildebrand, P.H. and Ackerman, B. 1984. Urban effects on the convective boundary layer. *J. Atmos. Sci.*, 41, 76–91.
- Högström, U. 1988. Non-dimensional wind and temperature profiles. *Bound. Lay. Met.*, 42, 55–78.
- Holt, T. and Raman, S. 1988. A review and comparative evaluation of multilevel boundary layer parameterization for first-order and turbulent kinetic energy closure schemes. *Rev. Geophys.*, 26, 761–80.
- Holtstlag, A.A.M. and Niewstadt, F.T.M. 1986. Scaling the atmospheric boundary layer. *Bound. Lay. Met.*, 36, 201–209.
- Hsu, W.-R. and Sun, W.-Y. 1991. Numerical study of mesoscale cellular convection. *Bound. Lay. Met.*, 57, 167–86.
- Hunt, J.C.R. (ed). 1985. *Turbulence and Diffusion in Stable Environments*. Oxford University Press, Oxford, 319 pp.
- Hunt, J.C.R., Kaimal, J.C. and Gaynor, J.E. 1988. Eddy structure in the convective boundary layer – new measurements and new concepts. *Q. Jl R. met. Soc.*, 114, 827–58.
- Joffre, S.M. 1985. The structure of the marine atmospheric boundary layer. A review from the point of view of diffusivity, transport and deposition processes. *Tech. Rept. No. 29*. Finnish Meteorological Institute, Helsinki.
- Kaimal, J.C. 1988. *The Atmospheric Boundary Layer – Its Structure and Measurement*. Indian Institute of Tropical Meteorology, Pune, 115 pp.
- Kaimal, J.C. and Wyngaard, J.C. 1990. The Kansas and Minnesota experiments. *Bound. Lay. Met.*, 50, 31–47.
- Kazanski, A.B. and Monin, A.S. 1961. On the dynamic interaction between the atmosphere and the Earth's surface. *Izv. Acad. Sci. USSR, Geophys. Ser.*, no. 5, 514–15.
- Kondo, J. 1975. Air-sea bulk transfer coefficients in diabatic conditions. *Bound. Lay. Met.*, 9, 91–112.
- Kondo, J., Kanechika, O. and Yasuda, N. 1978. Heat and moisture transfers under strong stability in the atmospheric surface layer. *J. Atmos. Sci.*, 35, 1012–21.
- Kropfli, R.A. and Hildebrand, P.H. 1980. Three-dimensional wind measurements in the optically clear planetary boundary layer with dual-Doppler radar. *Radio Sci.*, 15, 283–96.
- Kumar, R. and Adrian, R.J. 1986. Higher-order moments in unsteady turbulent penetrative thermal convection. *J. Heat Transfer*, 108, 323–9.
- Kustas, W.P. and Brutsaert, W. 1986. Wind profile constants in a neutral atmospheric boundary layer over complex terrain. *Bound. Lay. Met.*, 34, 33–54.
- LeMone, M.A. 1980. The marine boundary layer. In *Workshop on the PBL* (J.C. Wyngaard (ed.)), Amer. Met. Soc., Boston, 182–231.
- Lenschow, D.H. 1974. Model of the height variation of the turbulence kinetic energy budget in the unstable planetary boundary layer. *J. Atmos. Sci.*, 31, 465–74.
- Lenschow, D.H. (ed). 1986. *Probing the Atmospheric Boundary Layer*. Amer. Met. Soc., Boston.
- Lenschow, D.H., Wyngaard, J.C. and Pennell, W.T. 1980. Mean-field and second-moment budgets in a baroclinic convective boundary layer. *J. Atmos. Sci.*, 37, 1313–26.
- Lenschow, D.H., Li, X.S., Zhu, C.J. and Stankov, B.B. 1988a. The stably stratified boundary layer over the Great Plains. I. Mean and turbulence structure. *Bound. Lay. Met.*, 42, 95–121.
- Lenschow, D.H., Zhang, S.F. and Stankov, B.B. 1988b. The stably stratified boundary layer over the Great Plains. II. Horizontal variations and spectra. *Bound. Lay. Met.*, 42, 123–35.
- Lettau, H. 1990. The O'Neill experiment of 1953. *Bound. Lay. Met.*, 50, 1–9.
- Lettau, H.H. and Dabberdt, W.F. 1970. Variangular wind spirals. *Bound. Lay. Met.*, 1, 64–79.
- Liu, W.T., Katsaros, K.B. and Businger, J.A. 1979. Bulk parameterization of air-sea exchanges of heat and water vapour including the molecular constraints at the interface. *J. Atmos. Sci.*, 36, 1722–35.
- Long, R.R. 1974. Mean stress and velocities in the neutral barotropic planetary boundary layer. *Bound. Lay. Met.*, 7, 475–87.
- Louis, J.F. 1979. A parametric model of vertical eddy fluxes in the atmosphere. *Bound. Lay. Met.*, 17, 187–202.
- McBean, G.A. (ed). 1979. The planetary boundary layer. *WMO Tech. Note 165*. WMO, Geneva, 201 pp.
- McIntosh, P.C. and Hubbert, G.D. 1992. Ocean winds for marine modelling. *Aust. Met. Mag.*, 40, 61–9.
- Manins, P.C. 1982. The daytime planetary boundary layer: a new interpretation of Wangara data. *Q. Jl R. met. Soc.*, 108, 689–705.
- Martin, T. and Bakan, S. 1991. Airplane investigation of a case of convective cloud bands over the North Sea. *Bound. Lay. Met.*, 56, 359–80.
- Mason, P.J. 1987. Diurnal variations in flow over a succession of ridges and valleys. *Q. Jl R. met. Soc.*, 113, 1117–40.
- Mason, P.J. 1988. The formation of areally averaged roughness lengths. *Q. Jl R. met. Soc.*, 114, 399–420.
- Mason, P.J. and Derbyshire, S.H. 1990. Large-eddy simulation of the stably-stratified atmospheric boundary layer. *Bound. Lay. Met.*, 53, 117–62.
- Mellor, G.L. and Yamada, T. 1982. Development of a turbulence closure model for geophysical fluid problems. *Rev. Geophys. Space Phys.*, 20, 851–75.
- Miller, M.J., Beljaars, A.C.M. and Palmer, T.N. 1992. The sensitivity of the ECMWF model to the parameterization of evaporation from the tropical oceans. *J. Climatol.*, 5, 418–34.

- Moeng, C.-H. 1984. A large-eddy-simulation model for the study of planetary boundary-layer turbulence. *J. Atmos. Sci.*, *41*, 2052–62.
- Moeng, C.-H. and Wyngaard, J.C. 1984. Statistics of conservative scalars in the convective boundary layer. *J. Atmos. Sci.*, *41*, 3161–9.
- Monin, A.S. and Obukhov, A.M. 1954. Basic turbulent mixing laws in the atmospheric surface layer. *Tr. Geofiz. Inst. Akad. Nauk. SSSR*, *24*, 163–87.
- Monin, A.S. and Yaglom, A.M. 1971. *Statistical Fluid Mechanics*, Vol. 1, (J.L. Lumley (ed.)), MIT Press, Cambridge, 769 pp.
- Monin, A.S. and Yaglom, A.M. 1975. *Statistical Fluid Mechanics*, Vol. 2, (J.L. Lumley (ed.)), MIT Press, Cambridge, 849 pp.
- Nicholls, S. and Readings, C.J. 1979. Aircraft observations of the structure of the lower boundary layer over the sea. *Q. Jl R. met. Soc.*, *105*, 785–802.
- Nieuwstadt, F.T.M. 1984. The turbulent structure of the stable, nocturnal boundary layer. *J. Atmos. Sci.*, *41*, 2202–16.
- Nieuwstadt, F.T.M. 1985. A model for the stationary, stable boundary layer. In *Turbulence and Diffusion in Stable Environments* (J.R.C. Hunt (ed.)), Oxford University Press, Oxford, 149–79.
- Nieuwstadt, F.T.M. and Van Dop, H. 1982. *Atmospheric Turbulence and Air Pollution Modelling*. D. Reidel Publishing Company, Dordrecht, 358 pp.
- Noilhan, J., Benach, B., Druilhet, A. and Duboscloud, G. 1982. Étude expérimentale de la couche limite au dessus d'un relief modéré proche d'une chaîne de montagne. Partie I: Influence sur l'écoulement du relief à moyenne et grande échelles. *Bound. Lay. Met.*, *24*, 395–414.
- Olesen, H.R., Larsen, S.E. and Hojstrup, J. 1984. Modeling velocity spectra in the lower part of the planetary boundary layer. *Bound. Lay. Met.*, *29*, 285–312.
- Panin, G.N. 1990. Some experimental results from studies of air-sea interactions. *Bound. Lay. Met.*, *50*, 147–52.
- Panofsky, H.A. and Dutton, J.A. 1984. *Atmospheric Turbulence*. Wiley-Interscience, New York, 397 pp.
- Panofsky, H.A., Tennekes, H., Lenschow, D.H. and Wyngaard, J.C. 1977. The characteristics of turbulent velocity components in the surface layer under convective conditions. *Bound. Lay. Met.*, *11*, 355–61.
- Paulson, C.A. 1970. The mathematical representation of wind speed and temperature profiles in the unstable atmospheric surface layer. *Jnl appl. Met.*, *9*, 857–61.
- Pennell, W.T. and LeMone, M.A. 1974. An experimental study of turbulence structure in the fair-weather trade wind boundary layer. *J. Atmos. Sci.*, *31*, 1308–23.
- Schmidt, H. and Schumann, U. 1989. Coherent structure of the convective boundary layer derived from large-eddy simulations. *J. Fluid. Mech.*, *200*, 511–62.
- Schumann, U. 1988. Minimum friction velocity and heat transfer in the rough surface layer of a convective boundary layer. *Bound. Lay. Met.*, *44*, 311–26.
- Smedman, A.-S. 1991. Occurrence of roll circulations in a shallow boundary layer. *Bound. Lay. Met.*, *57*, 343–58.
- Smith, S.D. 1988. Coefficients for sea surface wind stress, heat flux and wind profiles as a function of wind speed and temperature. *J. geophys. Res.*, *93*, 15467–72.
- Smith, S.D. 1989. Water vapor flux at the sea surface. *Bound. Lay. Met.*, *47*, 277–93.
- Sorbjan, Z. 1989. *Structure of the Atmospheric Boundary Layer*. Prentice-Hall, Englewood Cliffs, 317 pp.
- Spillane, K.T. and Hess, G.D. 1988. Fair weather convection and light aircraft, helicopter and glider accidents. *J. Aircraft*, *25*, 55–61.
- Stull, R.B. 1988. *An Introduction to Boundary Layer Meteorology*. Kluwer Academic Publishers, Dordrecht, 666 pp.
- Thompson, R.S. 1978. Note on aerodynamic roughness length for complex terrain. *Jnl appl. Met.*, *17*, 1402–1403.
- van Dop, H., De Haan, B.J. and Cats, G.J. 1980. Meteorological input for a three-dimensional medium range air quality model. *Proc. 5th International Clean Air Congress*, Rio de Janeiro, 481–4.
- Venkatram, A. 1988a. Dispersion in the stable boundary layer. In *Lectures on Air Pollution Modeling* (A. Venkatram and J.C. Wyngaard (eds)), Amer. Met. Soc., Boston, 229–65.
- Venkatram, A. 1988b. Topics in applied dispersion modeling. In *Lectures on Air Pollution Modeling* (A. Venkatram and J.C. Wyngaard (eds)), Amer. Met. Soc., Boston, 267–324.
- Viney, N.R. 1991. An empirical expression for aerodynamic resistance in the unstable boundary layer. *Bound. Lay. Met.*, *56*, 381–93.
- Wayland, R.J. and Raman, S. 1989. Mean and turbulent structure of a baroclinic marine boundary layer during the 28 January 1986 cold-air outbreak (GALE 86). *Bound. Lay. Met.*, *48*, 227–54.
- Webb, E.K. 1970. Profile relationships: the log-linear range and extension to strong stability. *Q. Jl R. met. Soc.*, *96*, 67–90.
- Webb, E.K. 1977. Convection mechanism of atmospheric heat transfer from surface to global scales. *Proc. Second Australasian Conf. Heat and Mass Transfer*, University of Sydney, 523–39.
- Webb, E.K. 1984. Temperature and humidity structure in the lower atmosphere. In *Geodetic Refraction – Effects of Electromagnetic Wave Propagation through the Atmosphere*. (F.K. Brunner (ed.)), Springer-Verlag, Berlin, 85–141.
- Weil, J.C. 1988. Dispersion in the convective boundary layer. In *Lectures on Air Pollution Modeling* (A. Venkatram and J.C. Wyngaard (eds)), Amer. Met. Soc., Boston, 167–227.
- Wieringa, J. 1986. Roughness-dependent geographical interpolation of surface wind speed averages. *Q. Jl R. met. Soc.*, *112*, 867–89.
- Williams, A.G. 1991. Internal structure and interactions of coherent eddies in the lower convective boundary layer. Ph.D. dissertation. School of Earth Sciences, Flinders University, Bedford Park, SA.
- Williams, A.G. and Hacker, J.M. 1992. The composite shape and structure of coherent eddies in the convective boundary layer. *Bound. Lay. Met.* (in press).
- Willis, G.E. and Deardorff, J.W. 1974. A laboratory model of the unstable planetary boundary layer. *J. Atmos. Sci.*, *31*, 1297–1307.
- Wippermann, F. 1973. *The Planetary Boundary Layer of the Atmosphere*. Deutschen Wetterdienst, Offenbach, 346 pp.
- Wittich, K.-P. 1991. The nocturnal boundary layer over northern Germany: an observational study. *Bound. Lay. Met.*, *55*, 47–66.
- WMO. 1985. Report of the JSC/CAS Workshop on Modelling of Cloud Topped Boundary Layers. WMO World Climate Programme, *Rept. No. WCP-106*, WMO, Geneva, 26 pp. + appendixes.
- Wood, N. and Mason, P.J. 1991. The influence of static stability on effective roughness lengths for momentum and temperature. *Q. Jl R. met. Soc.*, *117*, 1025–56.
- Wu, J. 1980. Wind stress coefficients over sea surface from breeze to hurricane. *J. Phys. Oceanogr.*, *10*, 727–40.
- Wyngaard, J.C. 1983. Lectures on the planetary boundary layer. In *Mesoscale Meteorology – Theories, Observations and Models* (D.K. Lilly and T. Gal-Chen (eds)), Reidel, Dordrecht, 603–50.
- Wyngaard, J.C. (ed.) 1984. Large-eddy simulation: guidelines for its application to planetary boundary layer research. *Final Report 84101-GS-Z*, US Army Research Office, Research Triangle Park, NC, 122 pp.
- Wyngaard, J.C. 1985. Structure of the planetary boundary layer and implications for its modeling. *Jnl Clim. appl. Met.*, *24*, 131–42.
- Wyngaard, J.C. 1988a. Convective processes in the lower Atmosphere. In *Flow and Transport in the Natural Environment: Advances and Applications* (W.L. Steffen and O.T. Denmead (eds)), Springer-Verlag, New York, 240–269.
- Wyngaard, J.C. 1988b. Structure of the PBL. *Lectures on Air Pollution Modelling* (A. Venkatram and J.C. Wyngaard (eds)), Amer. Met. Soc., Boston, 9–61.

- Wyngaard, J.C. (ed.) 1990a. Atmospheric boundary-layer problems: A CAS Working Group report with contribution by J. Garratt, S. Panchev and V.N. Lykossov. *Long-Range Forecasting Research Rept. No. 11*, WMO/TD No. 334.
- Wyngaard, J.C. (ed.) 1990b. *Atmospheric boundary layer model evaluation workshop*. World Climate Programme Research, WCRP-42, WMO/TD-No. 378, 46 pp.
- Wyngaard, J.C. 1990c. Scalar fluxes in the planetary boundary layer – Theory, modeling, and measurement. *Bound. Lay. Met.*, 50, 49–75.
- Wyngaard, J.C. and Coté, O.R. 1971. The budgets of turbulent kinetic energy and temperature variance in the atmospheric surface layer. *J. Atmos. Sci.*, 28, 190–201.
- Wyngaard, J.C., Pennell, W.T., Lenschow, D.H. and LeMone, M.A. 1978. The temperature-humidity covariance budget in the convective boundary layer. *J. Atmos. Sci.*, 35, 47–58.
- Young, G.S. 1988a. Convection in the ABL. *Earth-Science Reviews*, 25, 179–198.
- Young, G.S. 1988b. Turbulence structure of the convective boundary layer. Part I: Variability of normalized turbulence statistics. *J. Atmos. Sci.*, 45, 719–26.
- Young, G.S. 1988c. Turbulence structure of the convective boundary layer. Part II: Phoenix 78 aircraft observations of thermals and their environment. *J. Atmos. Sci.*, 45, 727–35.
- Young, G.S. 1988d. Turbulence structure of the convective boundary layer. Part III: The vertical velocity budgets of thermals and their environment. *J. Atmos. Sci.*, 45, 2039–49.
- Zeman, O. 1981. Progress in the modeling of planetary boundary layers. *Ann. Rev. Fluid Mech.*, 13, 253–72.
- Zhang, S.F., Oncley, S.P. and Businger, J.A. 1988. A critical evaluation of the von Karman constant from a new atmospheric surface layer experiment. *Prepr. Eighth Symp. Turbulence and Diffusion, San Diego*, April 25–29, 1988, Amer. Met. Soc., Boston, 148–50.
- Zilitinkevich, S.S. 1972. On the determination of the height of the Ekman boundary layer. *Bound. Lay. Met.*, 3, 141–5.
- Zilitinkevich, S.S. 1989. Velocity profiles, the resistance law and the dissipation rate of mean flow kinetic energy in a neutrally and stably stratified planetary boundary layer. *Bound. Lay. Met.*, 46, 367–89.

